Landslide Regime Shift Detector (LRSD) for Landslide Early Warning Systems

Lorenzo Nava[a], Antoinette Tordesillas[b], Guoqi Qian[b], Filippo Catani[a]

[a] Machine Intelligence and Slope Stability Laboratory, Department of Geosciences, University of Padova, Padova, Italy.

[b] School of Mathematics and Statistics, University of Melbourne, Melbourne, VIC, Australia

---

This manuscript is a preprint and will be shortly submitted for publication to a scientific journal. As a function of the peer-reviewing process that this manuscript will undergo, its structure and content may change. If accepted, the final version of this manuscript will be available via the 'Peer-reviewed Publication DOI' link on the right-hand side of this webpage. Please feel free to contact any of the authors; we welcome feedback.

Corresponding author: Lorenzo Nava, lorenzo.nava@phd.unipd.it

Abstract: This research presents the development of a Landslide Regime Shift Detector (LRSD) which integrates advanced prediction models to provide insights into regime shifts within substantial landslide bodies. Our primary focus lies in the identification of these shifts, emphasizing that LRSD does not merely detect accelerations but discerns exceptional accelerations, defined in our context as deviations significantly departing from historical relationships between predictions and actual accelerations. The study focuses on slow-moving landslides, employing a Vector Error-Correction Cointegration (VECC) model to predict displacement at several monitoring points, with rainfall as a crucial influencing factor. While the VECC model effectively predicts rainfall-triggered accelerations, certain situations exhibit unexpected acceleration magnitudes, resulting in extreme residuals. To establish the LRSD, 24-hour aggregated residuals between predicted and observed displacements are employed. Kernel density estimation (KDE) is applied to derive cumulative distribution function (CDF) values for the residuals, with a predetermined threshold of 0.999 CDF triggering alerts for each monitoring point independently. A last step, which includes the persistence in time of the threshold exceedance and the number of monitoring points that exceed the threshold at the same time is performed. This is to reduce the effect of noisy displacement time series and to encode the "group dynamics," crucial for identifying pre-failure indications. This approach offers several advantages, including the effective identification of critical time states, adaptability, and transferability. Furthermore, it introduces novel information into local landslide early warning systems (Lo-LEWS), which consists of strong changes in landslide trends and anomalous responses to external triggers, if any. This approach significantly enhances confidence in the resultant alert, particularly when integrated with conventional alert systems, thereby improving the reliability of Lo-LEWS.

Keywords: landslide hazard; early warning; alert systems; autoregressive models; regime shifts.

Highlights

- Ground-based monitoring systems provide high-frequency landslide displacement observations.
- Vector Error-Correction Cointegration (VECC) model allows for space-time landslide displacement prediction.
- Differences between predicted and measured displacement uncover landslide regime changes.
- Landslide Regime Shift Detector (LRSD) delivers timely alerts in case of regime changes.

Graphical Abstract

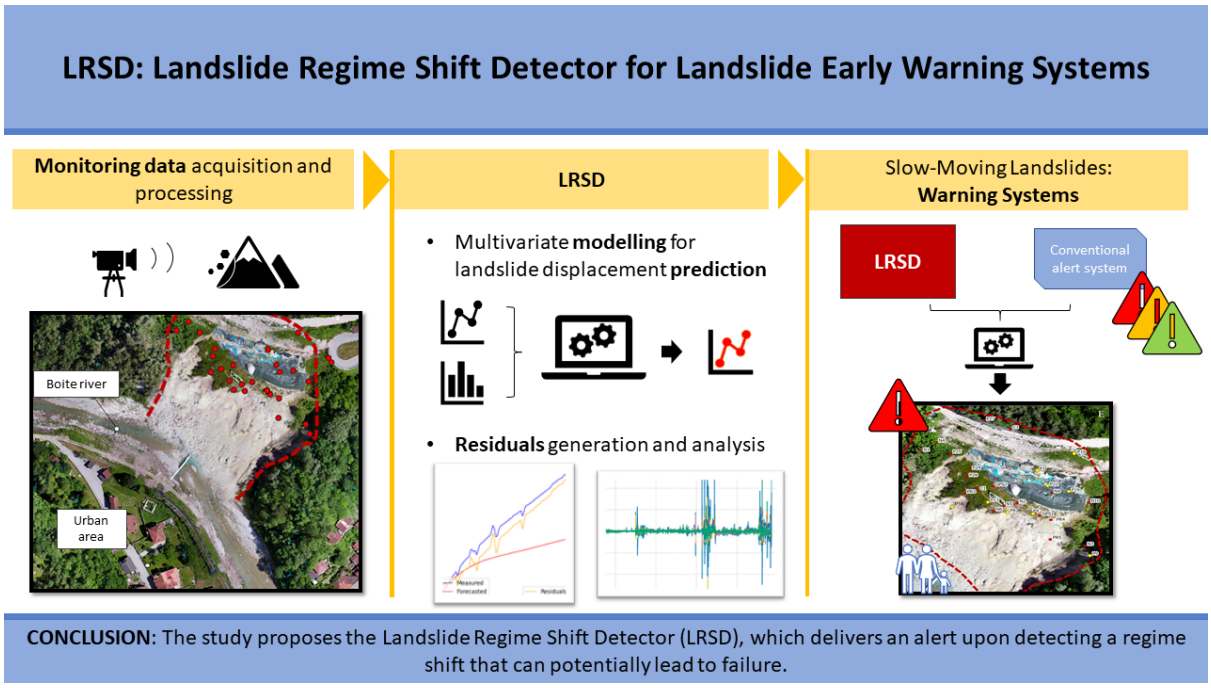

1. Introduction

Landslides are a common worldwide geohazard responsible for many casualties and economic losses each year (Froude and Petley, 2018). Although real-time monitoring of catastrophic landslides poses challenges, studying non-catastrophic, slow-moving landslides offers a valuable opportunity. These landslides exhibit downslope movement over extended periods, ranging from months to centuries, with rates spanning from millimeters to several meters per year (Lacroix et al., 2020). While slow-moving landslides typically do not result in fatalities, the potential for fast-moving debris flows originating within the slow-moving mass presents a threat to large areas (Palmer, 2017). Additionally, slow-moving landslides can undergo rapid acceleration, leading to catastrophic failures and widespread devastation. Notably, retrospective analysis has identified slow ground motions as precursory signals before catastrophic landslides occur. Consequently, the early detection of landslides before catastrophic events is a crucial focus in current research (Lacroix et al., 2020).

Landslide risk reduction employs various methods, broadly categorized into two approaches: structural measures that actively reduce landslide occurrence likelihood or engineering measures that enhance the resilience of at-risk elements, alongside non-structural strategies. Within the latter, landslide early warning systems (LEWS) have gained prominence globally for several reasons. They offer economic and environmental advantages over structural alternatives, utilize advancing monitoring technologies, and rely on reliable databases for model calibration (Intrieri et al., 2012; Pecoraro et al., 2019). The goal of LEWS is to decrease the risk of loss of life and other adverse impacts by providing timely information to individuals, communities, and organizations threatened by landslides, allowing them to prepare and take appropriate action.

LEWS can be deployed at two scales: local (Lo-LEWS) for addressing individual slope-level landslides (Dick et al., 2015) and territorial for regional-scale coverage (Segoni et al., 2014). Early warning systems are thought to be cost-effective in terms of risk reduction and damage mitigation (Intrieri et al., 2012). These systems include monitoring, forecasting, warning, and response tasks. To establish effective Lo-LEWS for large and complex landslides, it is essential to identify specific threshold values for key indicators. These indicators often include displacement, displacement rate, rainfall (such as intensity and duration), as well as pore water pressure or piezometric level (Crosta et al., 2017). These threshold values serve as critical benchmarks for triggering warning signals and informing decision-making processes to mitigate potential risks and damages associated with landslides. The most common approach to Lo-LEWS is the use of velocity thresholds, which are typically derived from historical data and reflect the displacement rates that have resulted in the past (Crosta and Agliardi, 2002). A comprehensive study by Pecoraro et al. (2019), after analyzing 29 Lo-LEWS, highlights that the warning models predominantly focus on displacement metrics, such as movement rate, velocity, and acceleration, due to their direct correlation with landslide activity (Festa et al., 2023). Meteorological factors are also considered in the models due to the prevalence of weather-induced landslides. Most systems also monitor parameters not directly included in the warning models, reflecting a proactive approach by managers to continuously assess and potentially update the adopted warning model over time.

The approaches based on displacement (and velocity) are grounded in the recognition that over an extended timeframe, observed slope displacements often conform to a standard creep curve. In this context, escalating displacements serve as a precursor indicating imminent failure (Fukuzono 1985; Kawamura 1985; Voight 1988; Zvelebill and Moser 2001). More recently, research has focused on the improvement of existing methods to pinpointing the precise time of failure (Segalini et al., 2018; Ju et al., 2020 Leinauer et al., 2023), yet an uncertainty persists regarding the appropriate timing for applying these methods. There remains a challenge in determining when to deploy such techniques, as they might be employed even when failure is not imminent, rendering them ineffective in such instances (Catani and Segoni, 2022).

The unpredictable nature of landslide progression, which is affected by various external variables, especially rainfall and reservoir water level changes, makes predicting landslide behavior complex. Recent advancements in landslide displacement prediction have demonstrated the efficacy of Artificial Intelligence (AI), specifically Machine Learning (ML) and Deep Learning (DL) techniques, which can accurately predict future velocity by taking contributing factors into account in addition to landslide displacement data. In the past decade, several AI-based techniques have been developed and tested for landslide displacement prediction. These techniques include various Machine Learning models such as artificial neural networks (Du et al., 2013), support vector machines (Han et al., 2021; Zhang and Li, 2014; Zhu and Hu, 2012), Gaussian process (Liu et al., 2014) and extreme

learning machine (Wang et al., 2019; Zhou et al., 2018), as well as several deep learning models (Gao et al., 2022; Nava et al., 2023; Zhang et al., 2022).

However, fine-tuning the parameters of these models to achieve the best performance often involves multiple iterations and extensive computational resources. This can hinder their real-time applicability, particularly in scenarios where rapid decision-making is crucial. Additionally, the static nature of these models poses limitations in adapting to dynamic changes in landslide behavior (Nava et al., 2023). Landslide patterns and environmental conditions can evolve due to various factors, such as changing weather patterns, human activities, and above all, geomechanical changes within the landslide body (Marmoni et al., 2023; Petley and Allison, 1997; Ye et al., 2022). Traditional forecasting models, once trained and optimized, do not readily accommodate these dynamic changes without undergoing a retraining process. This lack of adaptability becomes particularly relevant in the context of landslides, where timely and accurate predictions are vital for risk management and early warning systems (Intrieri et al., 2013). Landslide behavior can exhibit regime shifts or sudden anomalies that may not be adequately captured by a static model. Thus, there is a need for more flexible and agile approaches that can accommodate changes in behavior and conditions without the need for extensive retraining.

Currently, statistical vector autoregressive (VAR) time series models are emerging as viable solutions to overcome these limitations (Wang et al., 2020). These models have demonstrated effectiveness in predicting landslide displacement and providing early warnings. For instance, Qian et al. (2021) tackled the nonstationary and nonlinear characteristics of landslides by employing error-correction cointegration (ECC) and vector autoregression (VAR) techniques to manage non-stationarity. Similarly, Zheng et al. (2023) use ECC-VAR while also considering the nonlinear trend present in the high-dimensional vector time series data. The integration of these models in an augmented intelligence platform for what-if scenario analytics in Tordesillas et al. (2023) demonstrates its promise for near-real-time decision support in early warning and risk mitigation of catastrophic slope failure.

In this research, we propose a Landslide Regime Shift Detector (LRSD), wherein the difference between the measured displacement and the predicted displacement, known as residual displacement, is utilized to issue alerts. The vector error-correction cointegration (VECC) model was adopted to fit the spatiotemporal dependencies of the landslide displacement data and predict future displacements using rainfall as a triggering factor (exogenous variable). Given the hypothesized VECC model cannot fully capture the stronger and unexpected changes in the landslide trend, the residual displacement was employed to create a warning service that would alert authorities in the event of a sudden substantial alteration in the landslide pattern (when the model underestimates the displacement).

2. Case studies

Three different study cases are used in the research to evaluate the proposed LRSD. The Sant'Andrea landslide is located in the Dolomites, an area of the Southern-Eastern Italian Alps, in the Province of Belluno (Veneto Region, NE Italy), in Perarolo di Cadore municipality. The Pomarico landslide is located in the Basilicata Region, Southern Italy. The Veslemannen landslide is located in Romsdalen, Western Norway.

2.1 Sant'Andrea landslide

The Sant'Andrea landslide, located in the Dolomites area of the Southern-Eastern Italian Alps, affects the left-hand slope of the valley overlooking the Boite river, just upstream of the Perarolo village (see Figure 1). The position of the landslide is particularly hazardous for the inhabitants of the area, as a potential collapse of the unstable mass could lead to temporary damming on the Boite river, causing downstream flooding. The geological characteristics of the landslide area have been extensively studied over several years through various surveys that combined on-site investigations, geological and geotechnical analyses, and spatially distributed information on lithological units. The Sant'Andrea landslide is composed of a 30 m thick deposit of clay-calcareous debris, consisting of heterogeneous materials with varying grain sizes and geotechnical characteristics, sliding across the weathered part of the bedrock made up of a dolomitic lithology and folded layers rich in anhydrides and gypsum.

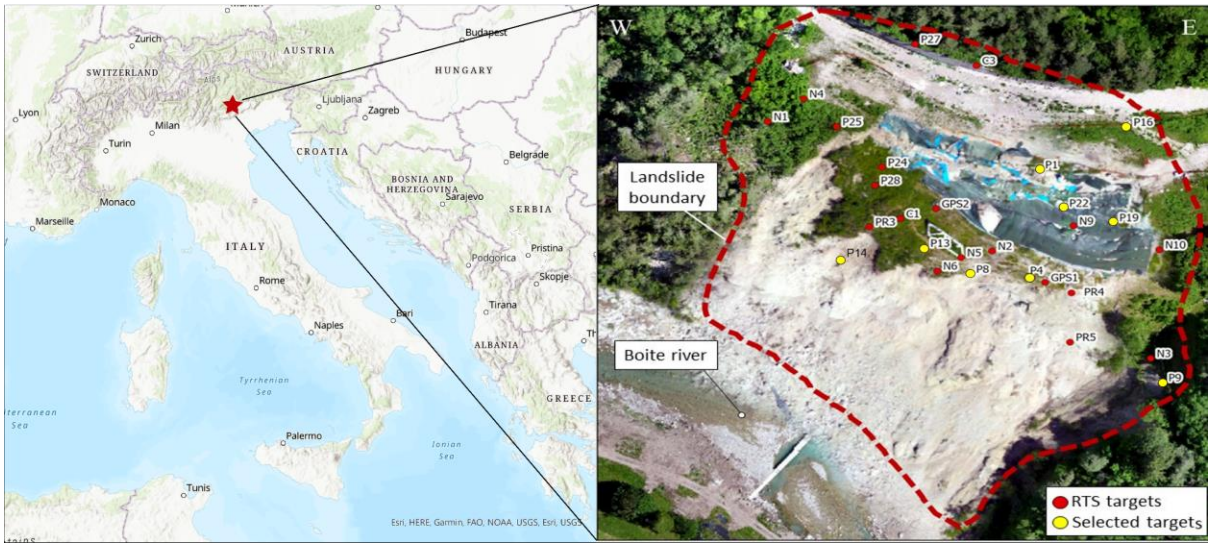

Figure 1. *Sant'Andrea landslide site. In the orthophoto, the targets of the topographic monitoring system and the boundary of the unstable area are shown.*

The Sant'Andrea landslide exhibits a complex behavior characterized by phases of slow and fast displacements, with the latter triggered primarily by prolonged and intense rainfall events. The geological and hydrogeological setting of the unstable slope was characterized through several surveys, which provided valuable information on the distribution of lithological units and aided in the interpretation of its behavior. Two groundwater flow systems were identified within the landslide: a shallow one in the upper layers of the debris deposits and a deep one involving the upper part of the bedrock, mainly composed of altered and fractured gypsum. Water plays a crucial role in triggering slope instability, both through the acceleration of displacements during rainfall events and the slow displacements induced by the active and deep circulation of water from the upper part of the slope in dry periods. The physical and chemical interaction between water and gypsum components of the upper part of the bedrock and the surficial debris layers influences the mechanical properties of the rock mass, with hydration processes causing plastic rheology of the weak gypsum lithology and the development of karst cavities and microcracks (Brezzi et al., 2021).

The Sant'Andrea landslide has been monitored since 2013 using a topographic system consisting of a Robotic Total Station (RTS) and reflective targets installed on the unstable slope. For this study, the P1, P4, P8, P9, P13, P14, P16, P19, and P22 targets were chosen since active monitoring points from 2013 to a minor landslide failure occurred on the 9th June 2021 in the area on which P14 was located. Six of them (P4, P8, P13, P14, P19, and P22) are located in an area affected by significant displacements, while the remaining three are located in stable areas. Figure 2 shows the measured cumulative displacement of the modeled monitoring points, along with hourly rainfall measured by a nearby rain gauge.

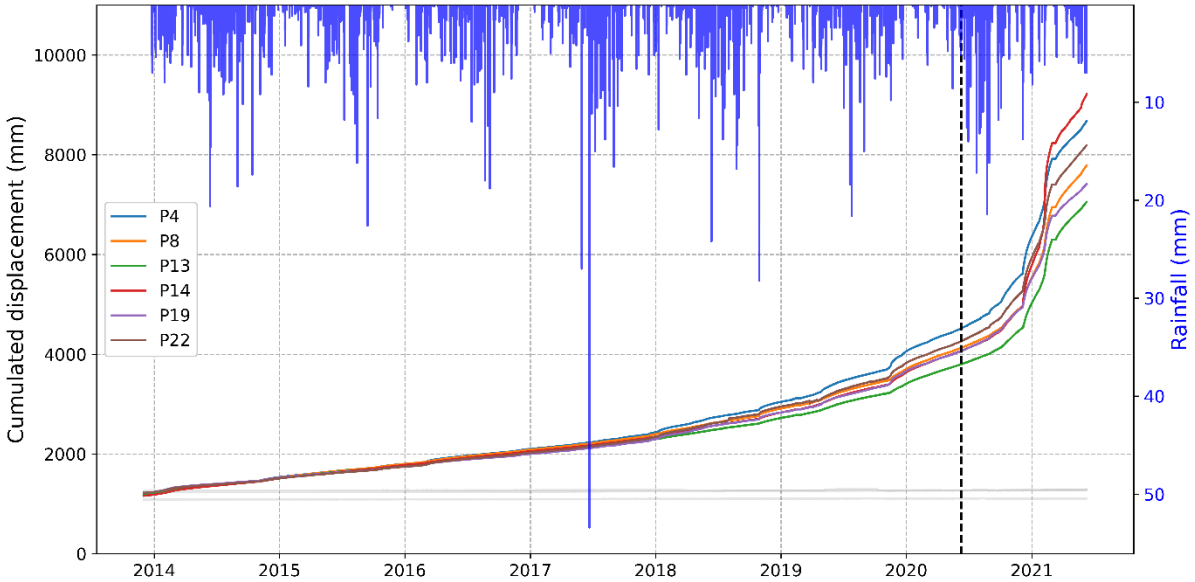

Figure 2. *Measured cumulated displacement of the modeled 9 monitoring points along with the rainfall in the Sant'Andrea landslide. All the time series have an hourly frequency. The three gray time series are the three stable points while the vertical black line divides the calibration set (left) and the test set (right).*

2.2 Pomarico landslide

The village of Pomarico is situated atop a narrow ridge at approximately 450 meters above sea level. In January 2019, Pomarico's southwestern urban area experienced a significant mass movement triggered by prolonged rains (see Figure 3). This event led to the collapse of a bulkhead supporting the main town road, resulting in the destruction and damage of private and commercial buildings, as well as widespread evacuation. The slope in this area is marked by various landforms related to old landslides, including scarps and depressions, covered partially with sandy-clayey debris containing dislodged blocks. Both sides of the slope adjacent to the investigated landslide feature ancient and recent landslide bodies. The geomorphological features indicate the reactivation of past landslide events, including those from 1959 and 1960, involving roto-translational sliding movements and earth flows. The 24–25 January 2019 rainfall event significantly altered water content and geomechanical conditions within the slope. This led to the activation of an earthflow on January 25, which in turn triggered retrogressive roto-translational sliding on January 29 (Doglioni et al., 2020). The latter was initially blocked by a bulkhead, but its deformation led to the slope's decompression and the progression of the roto-translational slide. The geological composition of the Pomarico southwestern slope is characterized by sandy and clayey deposits. The slope is covered by debris that incorporates tilted blocks of sandy-arenaceous layers, contributing to its complex nature. These deposits play a crucial role in the susceptibility to landslides, with variations in water content and geomechanical conditions significantly influencing slope stability. Additionally, the presence of ancient and recent landslide bodies further contributes to the complex behavior of the slope (Perrone et al., 2021). The combination of these geological features and material properties along with rainfall has a direct impact on the initiation and progression of mass movements in the area.

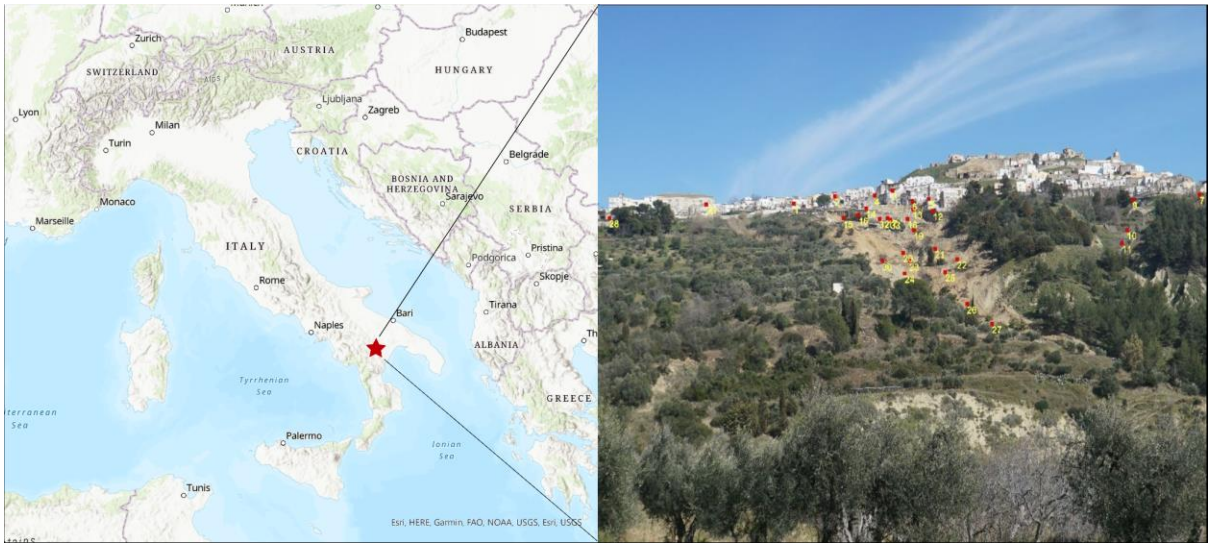

Figure 3. *Pomarico landslide site. In the orthophoto, the targets of the GB-SAR are shown.*

The Pomarico landslide has been monitored since 2019 using a ground-based synthetic aperture radar (GB-SAR). For this study, all 33 monitoring points were chosen. Ten of them (17, 18, 19, 20, 21, 23, 30, 31, 32, 33) are located in areas affected by significant displacements, while the remaining are located in relatively stable areas. Figure 4 shows the cumulative displacement of the monitoring points along with the rainfall measured by a nearby rain gauge.

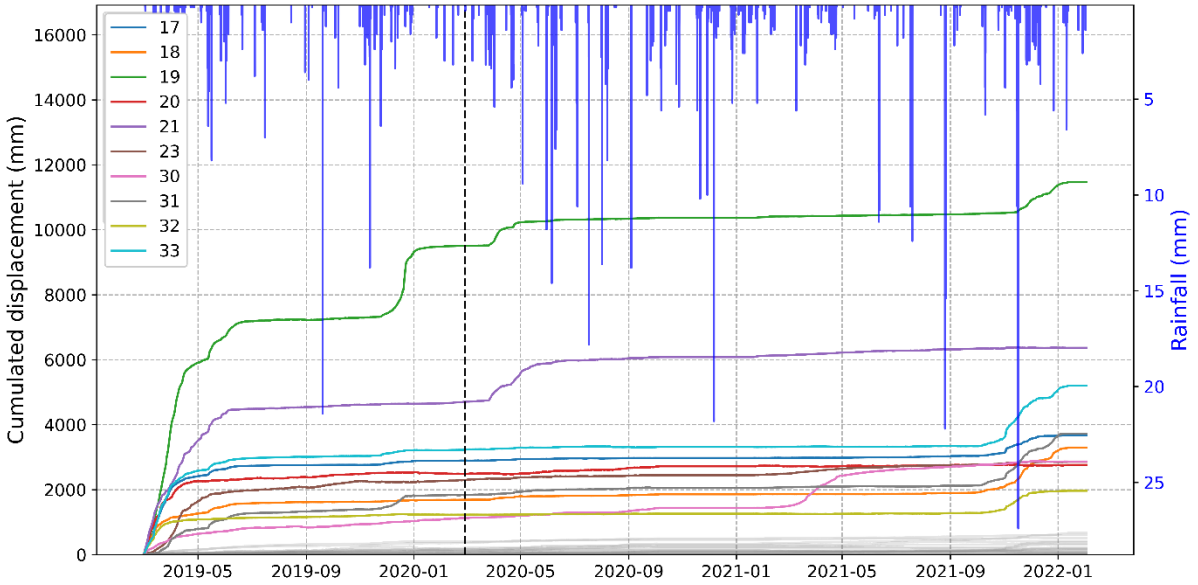

Figure 4. *Measured cumulated displacement of the modeled 33 monitoring points along with the rainfall for the Pomarico landslide. All the time series have an hourly frequency. The 23 gray time series are the stable points while the vertical black line divides the calibration set (left) and the test set (right).*

2.3 Veslemannen landslide

The Veslemannen unstable rock slope was located in Romsdalen, Rauma Municipality, Western Norway. Romsdalen is a 30-kilometer-long U-shaped glacial valley carved into the crystalline basement of the Western Gneiss Region, which underwent metamorphism during the Caledonian orogeny (Saintot et al., 2012). The ice sheet in the area began to thin around 15–13 thousand years ago, with a valley glacier extending to the fjord during the Younger Dryas period. The Mannen unstable rock slope, where Veslemannen was located, consists of highly folded and deformed high-grade metamorphic rocks. These rocks exhibit gravitational fracture opening along an east-west sub-vertical foliation and nearly north-south fractures. Different mechanisms of deformation were proposed for Mannen, including translational sliding and wedge failure with steps along the sliding surface. The

structural and topographic conditions in the area make it prone to slope collapses, and Romsdalen valley has a high density of post-glacial rock slope failures in Norway. The slope angle of Veslemannen ranged from 45 to 50 degrees, with a steeper frontal part at 70 degrees (Hilger et al., 2018). The upper part was highly fractured with loose blocks, while the middle part contained crushed rock. The lower part, or toe area, consisted of more intact rock and included a pinnacle known as "Spiret" or "the Tower," which was considered a key block stabilizing the upper part of the slope. The rockslide upper boundary was located at 1220 meters above sea level, marked by a snow-filled open fracture. Most of the movement and the final failure of Veslemannen occurred along one of the parallel transverse fractures below the back fracture. The estimated volume of Veslemannen was approximately 120,000–180,000 cubic meters, but the failure in September 2019 involved only 54,000 cubic meters.

Figure 5. *Veslemannen rockslide site. Photo from Kristensen et al., (2021).*

The rockslide was continuously monitored with real-time instrumentation and monitoring initiated in 2009. Various instruments, including GNSS antennas, lasers, extensometers, tiltmeters, borehole instrumentations, web cameras, a meteorological station, and ground-based interferometric radar systems, were used. For the validation of the proposed LRSD, we use the high-frequency GB-SAR monitoring system. The radar was continuously in place from October 6, 2014, from the valley floor at Lyngheim. 7 out of the 8 monitoring points are located in the failed area. For further information about the rockslide please refer to Kristensen et al., (2021).

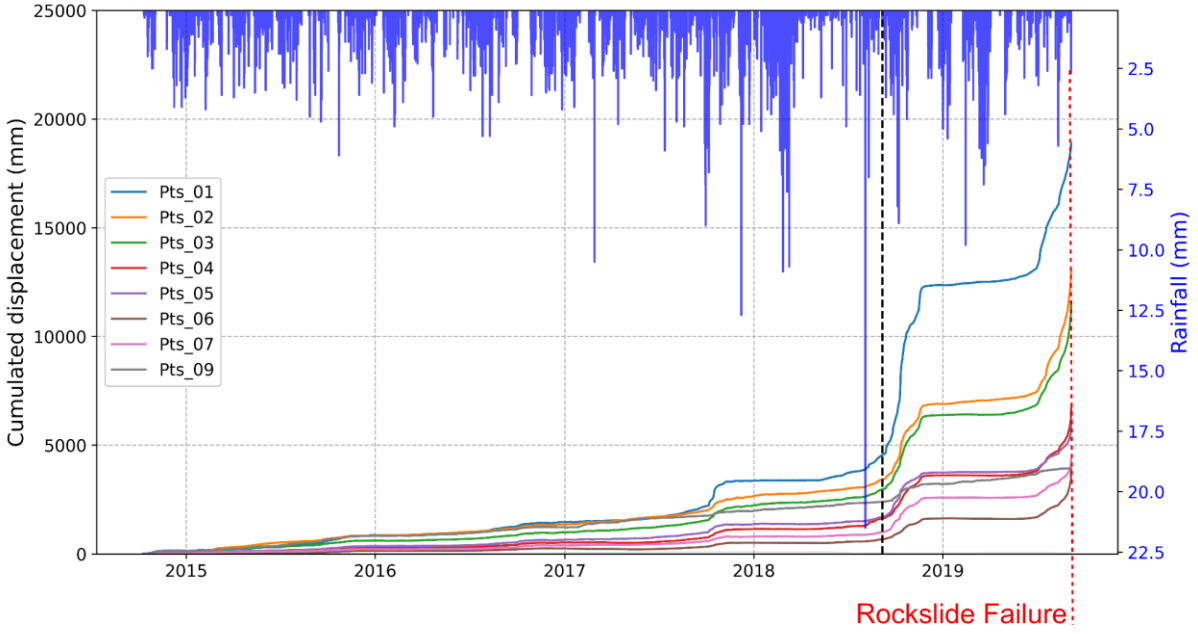

Figure 6. *Measured cumulated displacement of the modeled 9 monitoring points along with the rainfall. All the time series have an hourly frequency. The gray time series is the stable point while the vertical black line divides the calibration set (left) and the test set (right). The failure occurred at the end of the plotted series.*

3. Methodology

The methodology of the proposed alert service is composed of two main steps: (i) model training and prediction, and (ii) alert threshold estimation based on the difference between the predicted and measured displacement (residuals). Figure 7 shows the overall methodology workflow.

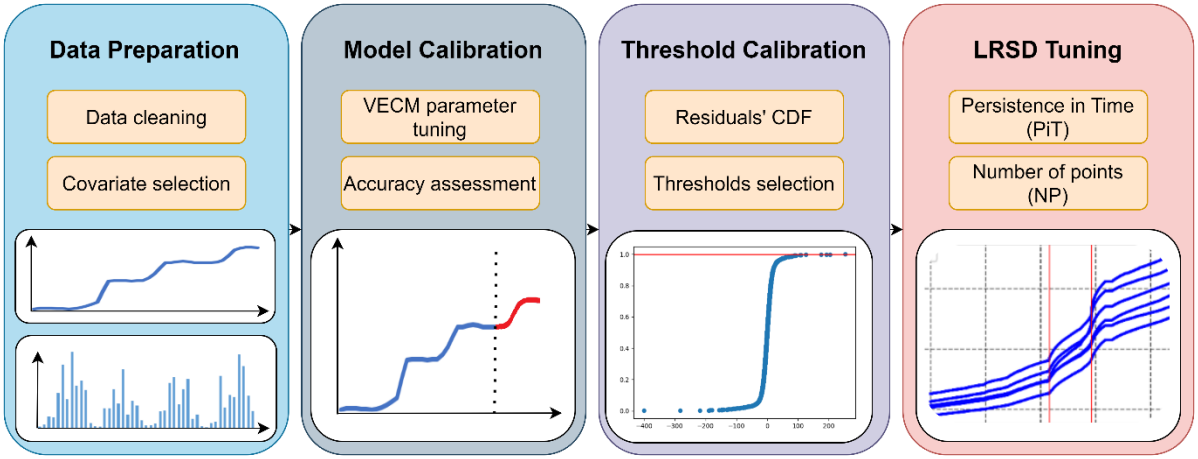

Figure 7. *Overall methodology workflow.*

3.1 Landslide Displacement Prediction

The data-driven VECC model is designed to "learn" and adapt to the changing ground conditions. This is achieved by incorporating historical displacement data, consisting of displacement time series across multiple locations, coupled with an important exogenous variable—rainfall, which has been identified as the primary factor triggering landslide accelerations in the considered cases.The VECC model is used to forecast the displacement of all monitoring points of the landslides simultaneously. The VECC model is a multivariate time series model that allows for the analysis of the long-term relationships among variables (Wang et al., 2020).

$$\Delta y_t = \underbrace{\alpha(\beta' \ \eta')\begin{pmatrix} y_{t-1} \\ D_{t-1}^{co} \end{pmatrix}}_{\text{Error correction}} + \underbrace{\mathbf{\Gamma}_1 \Delta y_{t-1} + \cdots + \mathbf{\Gamma}_{p-1} \Delta y_{t-p+1}}_{\text{Lagged endogenous}} + \underbrace{\mathbf{\Upsilon}_1 \Delta x_{t-1} + \cdots + \mathbf{\Upsilon}_{p-1} \Delta x_{t-p+1}}_{\text{Lagged exogenous}} + \underbrace{u_t}_{\text{Error}} \quad (1)$$

where y_t is the Nx1 displacement at time *t* over N locations
$\Delta y_t = y_t - y_{t-1}$
Δx_t is an exogenous scalar variable at time *t*
D_{t-1}^{co} is function of *t* specified by *n*, *ci*, *li*
D_{t-1}^{co} = *1* If deterministic = *ci*
D_{t-1}^{co} = *t-1* If deterministic = *li*
D_{t-1}^{co} = 0 If deterministic = *n*
Γ_j is NxN matrix giving the impact of Δy_{t-j} on Δy_t, j = 1, 2 … p-1; estimated by the general least squares (GLS) method
Υ_j is NxN matrix giving the impact of Δx_{t-j} on Δy_t, j = 1, 2 … p-1; estimated by the GLS method
α is the adjacent matrix; estimated by the GLS method
β' is the cointegration matrix; estimated by the GLS method
η' is the deterministic trend; estimated by the GLS method

The implementation of the VECC model is carried out using the Python programming language, specifically leveraging the *statsmodels* (https://www.statsmodels.org) library for analysis (Lütkepohl, 2005). The calibration of the model is performed on a dataset comprising historical displacement data and corresponding rainfall data,

both of which are collected at an hourly frequency. To ensure the model's accuracy, an hourly forward validation technique is employed, allowing for rigorous validation. In this process, the model undergoes training, prediction (24 hours ahead), and validation steps, which are repeated for each hour within the calibration phase. The efficient processing time of less than one minute enables this repetitive procedure to be completed swiftly (refer to Figure 8). One notable feature of the prediction scheme is that the training set maintains a fixed-length training window that advances with time. As new data becomes available, the oldest data points are removed, ensuring that the model consistently learns from the most recent landslide states. This adaptability enables the model to adjust to any potential changes in landslide behavior, such as a regime shift to tertiary creep.

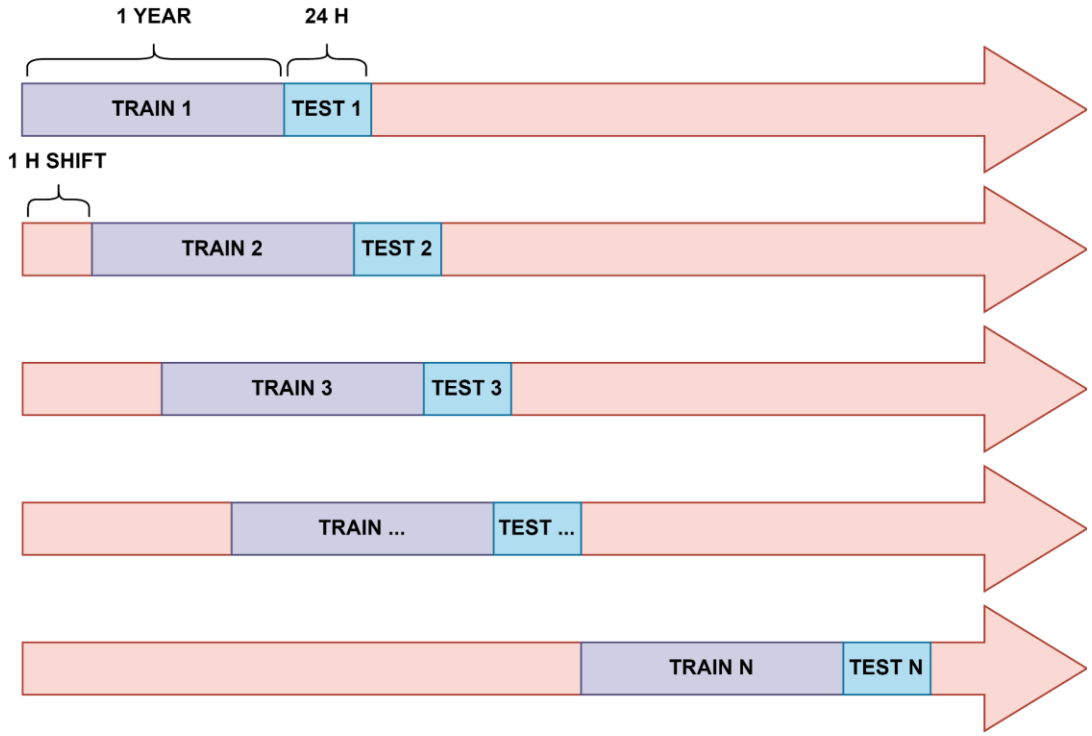

Figure 8. *Scheme of the predicting approach. The VECC model is re-trained every hour, and it forecasts 24 hours. The training length is one year. Training and testing are repeated shifting the window forward every hour.*

The use of the VECC model in this study allows for the simultaneous prediction of the displacement of multiple points on the landslide, which is important for the development of an effective alert system. By incorporating the exogenous variable of rainfall, into the model, the VECC approach provides a more accurate and reliable forecast of landslide activity, enabling more effective measures to be taken to mitigate the risks associated with the landslides. Ablation analysis on the best rainfall shifts has been conducted, as well as an accurate tuning of the model parameters, to obtain the best possible prediction by the model. The VECC model has undergone rigorous optimization and tuning using the calibration sets to ensure accurate prediction of rainfall-triggered accelerations. It's crucial to note that the VECC model doesn't inherently impose restrictions when predicting specific landslide velocities.

The hyperparameters we optimize by ablation, comparing the scores yielded by the forward validation over the calibration window, are time lag (p=2, 4, 6, 8, 10, 12, 14, 16, 18, 20, 24), and deterministic terms (no deterministic terms, constant term outside the cointegration relation, constant term within the cointegration relation, linear trend outside the cointegration relation, linear trend within the cointegration relation, and all the possible combinations of the above). The model parameters are estimated through the maximum likelihood estimation method. The time lag is the number of lagged differences to include in the model. This parameter determines the order of the autoregressive (AR) process for differenced data. In a VECC model, differenced variables are used to capture the short-term dynamics of the system due to they being stationary more likely. The D_{t-1}^{co} variable in the error-correction term incorporates deterministic effect into the model. And the other part in the error-correction term is to turn the non-stationary or trend-like patterns in endogenous (displacement) time series data into a stationary one. The cointegration rank is re-determined iteratively before every model training, by using the *select_coint_rank* function built within the *statsmodels* library, specifically for VECC models. Table 1 shows the

optimal parameters for each study case, along with the number of monitoring points and the number of observations.

It has demonstrated the ability to predict accelerations with precision in most cases, wherein it suggests the VECC model provides adequate characterization of the underlying landslide movement. However, there are certain instances where the model encounters unexpected magnitudes of accelerations that surpass the anticipated levels. Further examination of these instances reveals specific details that warrant closer attention. These details are discussed in the following subsections, providing a comprehensive understanding of the factors contributing to the model's occasional deviation from expected results. By delving into these specific instances, we can gain valuable insights into the underlying causes of the greater-than-anticipated accelerations. The data used for the calibration are the ones included in the calibration set (refer to Figures 2, 4, and 6). Over time, when the system encounters an unexpected (explosive) acceleration in landslide movement, it tends to underestimate the displacement initially. Subsequently, when this acceleration data is incorporated into the system's training set, the model adjusts to the evolving trend of the landslide. As a result, it tends to overestimate the displacement when the landslide's velocity decreases following the initial acceleration. This phenomenon accounts for the occurrence of both positive and negative spikes as observed in Figures 9, 13, and 17. This indicates a lack of the capability of the VECC model characterizing explosive nonstationarity and nonlinear effects from the exogenous variables. It is beyond the scope of this paper to develop a statistical model more advanced than the VECC model to possess this capability. Rather, we will exploit this lack of capability to develop a residual-based landslide alert system in the following subsections (Gouriéroux and Zakoïan, 2017; Phillips and Shi, 2020; Blasques et al., 2022; Phillips et al., 2011).

Table 1 Characteristics of the data series and optimal parameters for the VECC model, for the three modeled study cases.

Study Case	Number of monitoring points (Moving) (Failure)	Number of observations (Frequency)	Deterministic term	Time lag
Sant'Andrea	9 (6)(1)	66010 (1h)	n	6
Pomarico	33 (10)(0)	43090 (1h)	ci	10
Veslemannen	8 (7)(7)	25675 (1h)	li	4

3.2 Residual-based Landslide Alert System

The proposed early warning service relies on the residual values computed between the predicted and measured displacement of each point individually and it is built upon the method proposed by (Jiang and Chen, 2022). Specifically, the mean of the residuals is computed for each predicted 24-hour period. In other words, the difference between the predicted and observed values of displacement for each 24 hours is averaged to obtain the residual displacement. The early warning system then employs a kernel smoothing method to estimate the probability distribution underpinning these residuals. The estimate is nonparametric and non-normal and is named kernel density estimator (KDE)(Chen, 2017). The proposed alert system uses KDE to compute the cumulative distribution function (CDF) value of the residual at each monitoring point for each given time period. The CDF value at a monitoring point exceeding a critical threshold, e.g. 0.999, is an indication of that point being at risk of failure. It is shown that KDE can better fit the residuals resulting in a small number of false alerts (Jiang and Chen, 2022). Two different strategies to define the critical threshold were tested. The first consists of fitting the residual distribution and comparing the corresponding residual value to the 0.999 threshold of CDF every hour. The first workflow reduces the number of alarms consistently. However, the sensitivity of the threshold decreases sensibly after extreme residual values, as one extreme residual value might set a too high threshold. The consequence is that no alert is sent after relatively big residual values. Therefore, a second strategy (more conservative) which considers the historical residual distribution is adopted to set the thresholds which will be the same for all the testing sets (one year in each case). We consider the 0.999 CDF value as the threshold to be exceeded (> 0.999) to trigger an alert since we expect the most critical instances to be the ones in which our model heavily underestimates the landslide displacement (and not < 0.001 since we do not consider critical the case in

which the prediction overestimates the displacement). These values are commonly used in the literature (Jiang and Chen, 2022). The corresponding threshold value in the residuals is calculated based on the distribution of the residuals for the entire calibration window for each one of the monitoring points located in the unstable area (the moving ones), separately. This means that we will end up with a different residual threshold for each one of the moving monitoring points. To reduce the number of false alerts, persistence in time (PiT) and the number of points (NP) that exceed the threshold have been considered which can be tuned according to any specific case. A single point might randomly exceed the threshold due to occasional spikes of noise in the measured displacement. To mitigate the issue and propose an approach that can be tuned directly by the stakeholders according to the context in which the landslide is located, all the combinations from 1 to 25 consecutive hours are evaluated.

4. Results

We present results for both the model prediction outcomes and the final alert service for three different study cases. Results for each case study are displayed separately, thus providing valuable information about the performance and effectiveness of the implemented methods in the context of landslide prediction and early warning for each test site. The procedure is developed using the Python programming language. All experiments were conducted on a computer operating on the Windows system, equipped with a 3rd Gen Ryzen Threadripper 3990X CPU.

4.1 Sant'Andrea landslide

From 9th June 2020 to 9th June 2021 the landslide behavior changes substantially, showing sudden strong accelerations, and an overall increase in the displacement rate (Figure 2). This referenced year is used to assess the performance of the LRSD since we specifically aim to evaluate and analyze the behavior of the proposed service as well in landslides with strong dynamic behavior. The frequency of the time series analyzed is hourly, meaning that each test set, being one year is composed of 8760 time steps.

4.1.1 Model calibration and tuning

After the model is trained, it is used to predict the displacement of the 9 monitoring points on the landslide for 24h (of which 6 are consistently moving and 3 are in stable areas), considering the measured values of the exogenous variable, rainfall, for the entire prediction window. The predicted displacement values can then be compared to the actual displacement values to assess the accuracy of the model. In the reference year (9th June 2020 to 9th June 2021), it is evident how the residuals become unstable, especially for P14, which fails at the end of the plotted data (see Figure 2). Over time, when the system encounters an unexpected acceleration in landslide movement, it tends to underestimate the displacement initially. Subsequently, when this acceleration data is incorporated into the system's training set, the model adjusts to the evolving trend of the landslide. As a result, it tends to overestimate the displacement when the landslide's velocity decreases following the initial acceleration. This phenomenon accounts for the occurrence of both positive and negative spikes as observed in Figure 9.
In this case, the VECC model yielded optimal results with the following parameter settings: a detrending order of 0, lagged values of 6, and no deterministic terms ('*n*'). By excluding deterministic terms, the model assumes that the displacement behavior is solely determined by the historical relationships captured by the error correction mechanism. This implies that any other external or fixed effects that might affect the variables need not be considered or accounted for in the model. However, this model is valid for the displacement data series, and not for the exogenous rainfall.
The combined RMSE of the refined model across both the calibration and test sets amounts to 5.03 mm. This relatively high value is notably attributed to the landslide events observed in the past year (see Figure 2). Ablation analysis focusing on the external variable revealed that the most optimal outcomes (lowest RMSE) are obtained when considering rainfall from the current day up to 18 days prior.

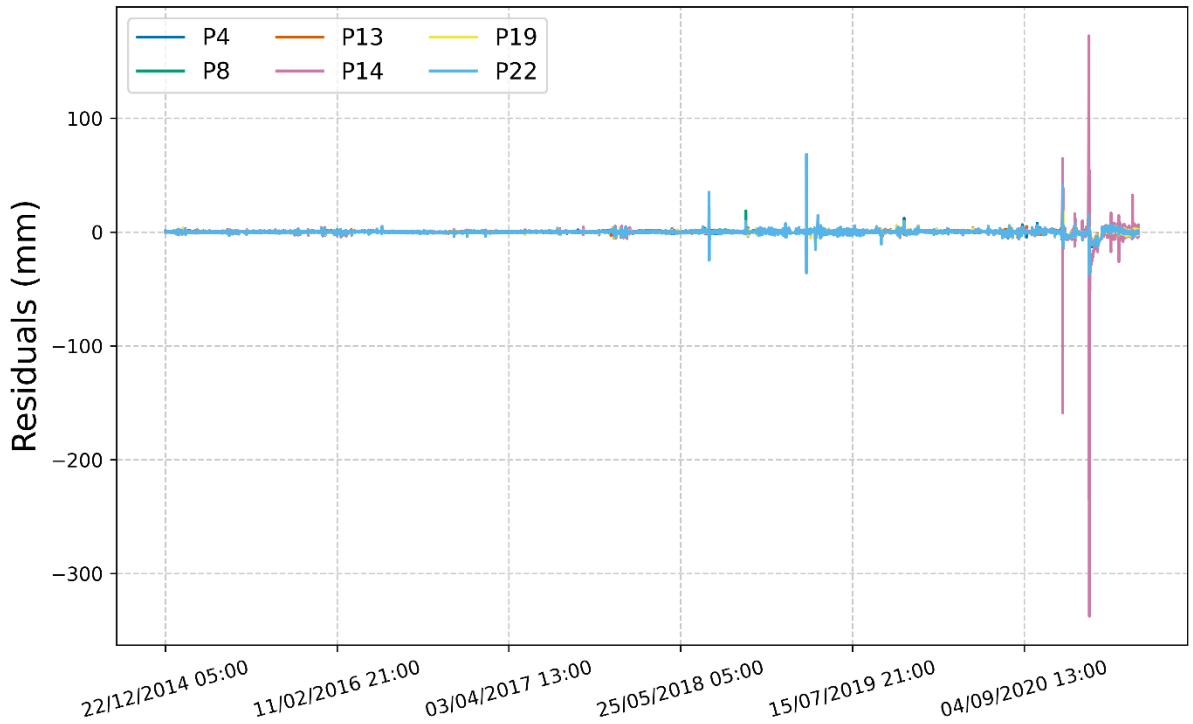

Figure 9. *Mean of residuals per 24h for the 6 monitoring points located in the unstable landslide area.*

4.1.2 Residual-based Landslide Alert System

We carefully analyze the distribution of average 24-hour differences leading up to June 9, 2021. This forms the core of our approach to trigger alerts in the year that follows. Within two critical accelerations, all six monitoring points have residuals consistently exceeding the predefined thresholds, proving that our approach for setting the thresholds is robust. Taking a closer look at the finer temporal details of the test year, we identify a recurring pattern where specific points sporadically surpass the established thresholds. Notably, during the evaluation year, P14 demonstrates recurrent instability. This instability continues throughout the entire year, resulting in a total of 380 instances where the threshold is exceeded. However, in the case of the Sant'Andrea landslide, the volume related to a single monitoring point does not consist of a dangerous situation for the Perarolo village.

An alert will be activated when the residuals exceed the threshold persistently across a pre-specified consecutive number of time intervals, i.e. PiT, and over a pre-specified number of monitoring points, i.e. NP. The frequency of alerts significantly decreases when the number of consecutive one-hour intervals considered increases. This phenomenon is depicted in Figure 10a, indicating that a significant proportion of alerts are sporadic rather than consistent. The noticeable drop in alert frequency as we extend the time period suggests that many alerts are not indicative of sustained trends but rather transient and irregular occurrences. In Figure 10b, we observe another noteworthy trend: the number of alerts decreases notably as the pre-specified number of monitoring points increases. This approach proves valuable in reducing false alarms, particularly in situations where a small number of monitoring points with volume-related risks are not a significant concern for the population's safety.

Figure 11 displays the raw alerts produced by the system for each unstable monitoring point, without accounting for PiT or NP. As evident in Figure 11, certain monitoring locations display numerous false alerts scattered throughout the entire testing dataset, with a concentration in the latter half of the year, particularly in P8, P13, and P14. When examining all the plots together, it becomes evident that some of these alerts pertain only to a small number of locations and do not accurately represent the entire landslide area. Therefore, additional filtering is required in this case. Figure 12 shows the effectiveness of considering the proposed combination between PiT and NP. The number of alerts significantly decreases, limiting them to the two most critical instances. It is not difficult to notice how the number of delivered alerts becomes acceptable after selecting NP=4 monitoring points altogether exceeding the threshold for PiT=3. However, it is generally preferable to opt for the lowest PiT to reduce the delay of the delivered alert.

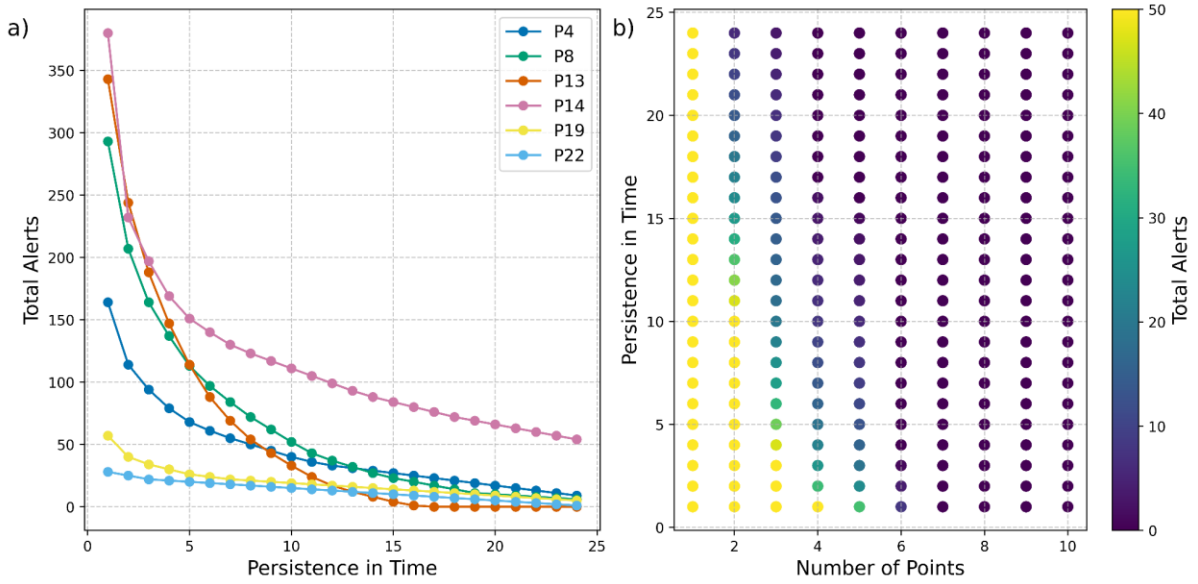

Figure 10. *a) Effect of the PiT on the number of times each monitoring point exceeds the threshold during the test year. b) Effect of the combination of PiT and the number of points that exceed the threshold simultaneously on the overall number of alerts the* LRSD *delivers.*

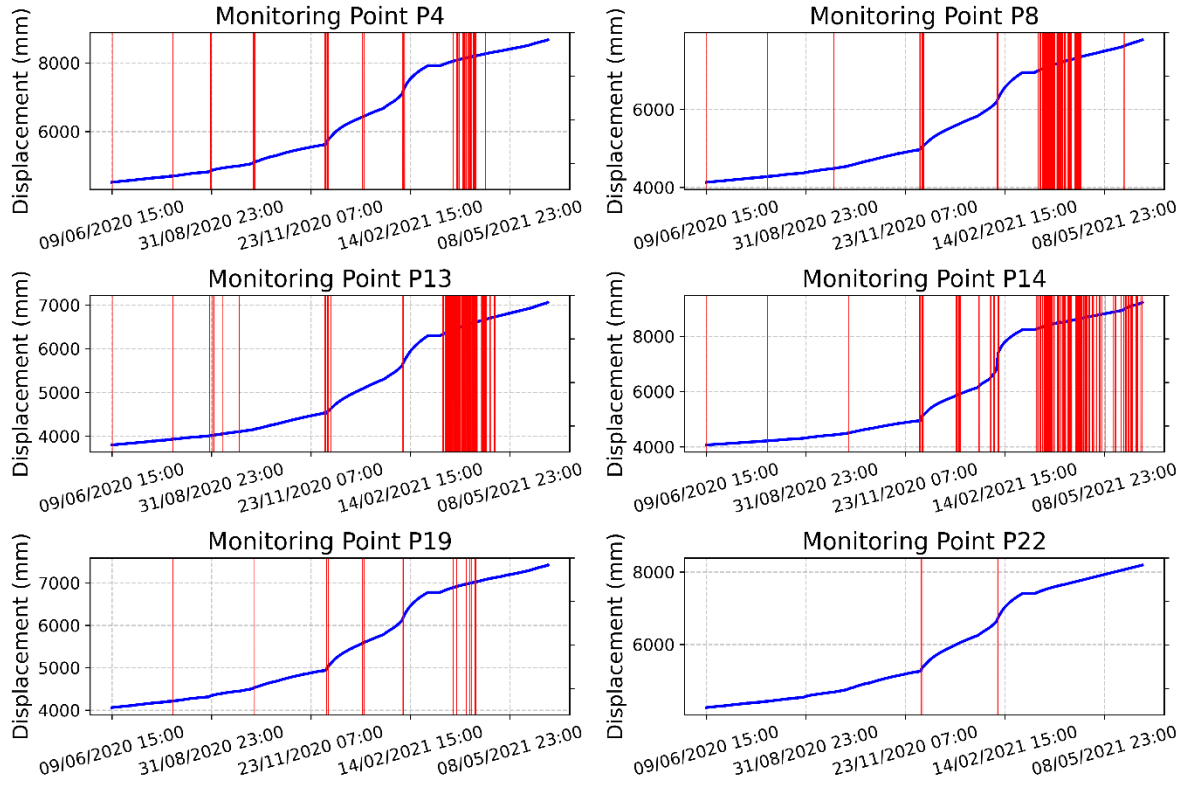

Figure 11. *Measured cumulative displacement (blue) and instances in which the threshold is exceeded for each monitoring point (red) located in the unstable landslide area.*

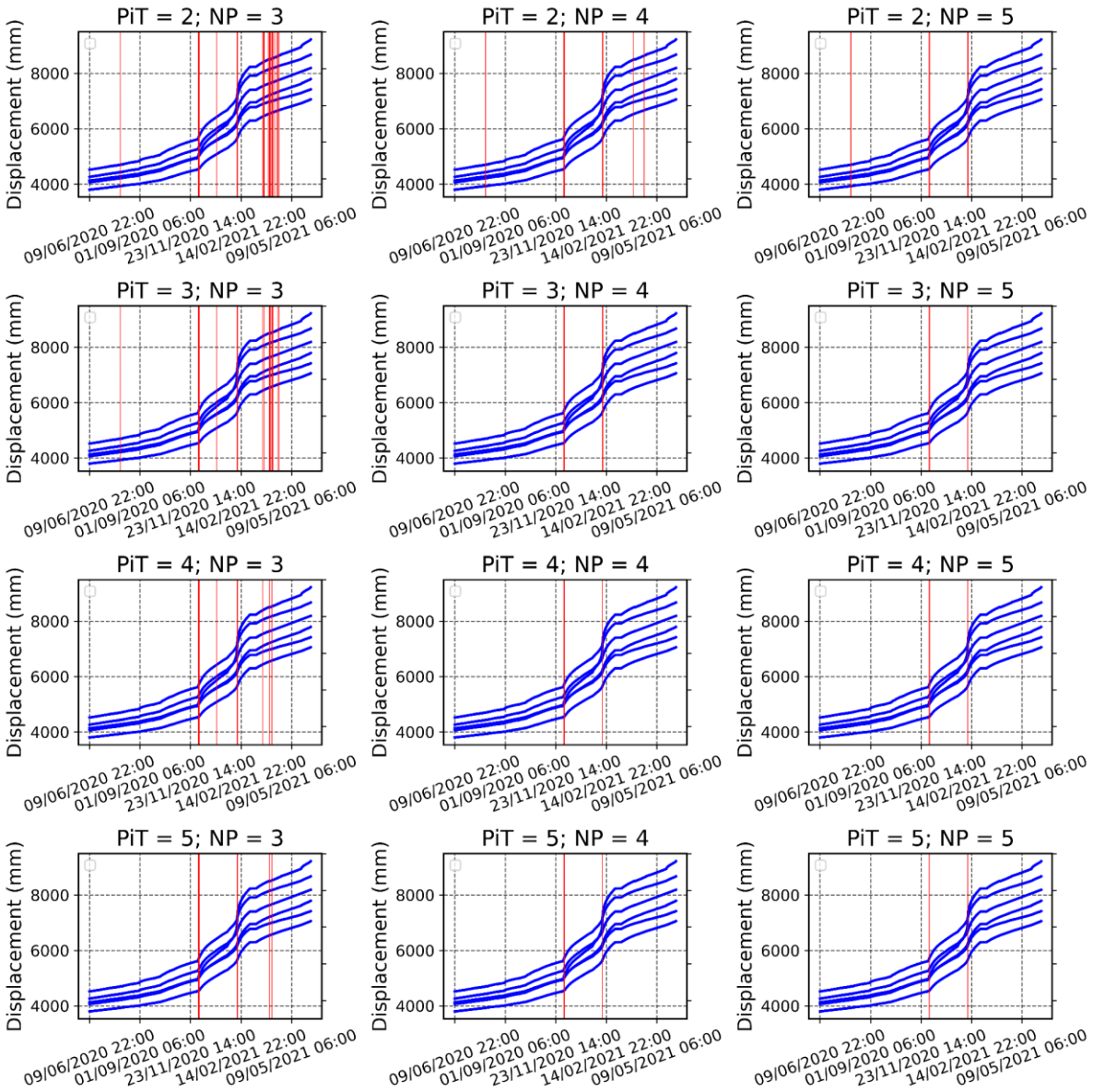

Figure 12. *Alerts (red) are delivered using 2, 3, 4, 5 as PiT and 3, 4, 5 as the number of points that exceed the threshold simultaneously. The measured cumulative displacement of the 6 points located in the unstable area is shown in blue.*

4.2 Pomarico landslide

The behavior of the Pomarico landslide remains relatively consistent between the calibration and test sets, unlike the observed variability in the Sant'Andrea landslide. In this scenario, we aim to assess the effectiveness of the proposed LRSD when the landslide's behavior remains relatively stable.

4.2.1 Model calibration and tuning

After the model is trained, it is used to predict the displacement of the 33 monitoring points on the landslide for the next 24h (of which 9 are consistently moving and 24 are relatively stable), considering the measured values of the exogenous variable, rainfall, for the entire prediction window. In this case, the calibration window is temporally smaller than the test set (see Figure 4). Again, the predicted displacement values can be compared to the actual displacement values to assess the accuracy of the model.

In this case, it can be seen how the residuals remain relatively stable for all the considered time series (see Figure 13). From September 2020 to January 2021 the magnitude of the residuals strongly decreased given some problems with the monitoring instrumentation. Just towards the end of the series, we can see some increase in

residual values, which become particularly unstable for monitoring point 33. In this case, the VECC model yielded optimal results with the following parameter settings: a detrending order of 0, lagged values of 10, and '*ci*' as a deterministic term. This means that the displacement has a linear trend. The combined RMSE of the refined model across both the calibration and test sets amounts to 0.12 mm. Ablation analysis focusing on the external variable revealed that the most optimal outcomes are obtained when considering rainfall from the current day up to 72 days prior (with a 3-day shift interval).

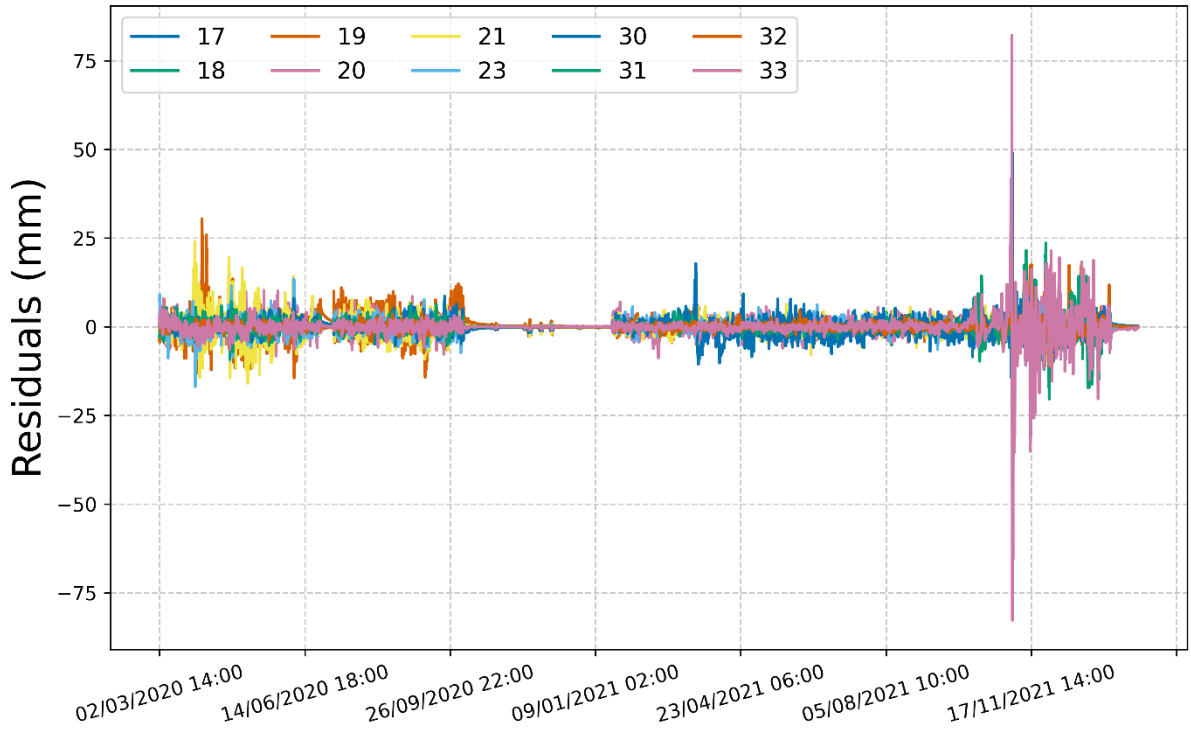

Figure 13. *Mean of residuals per 24h for each monitoring point located in the moving landslide area.*

4.2.2 Residual-based Landslide Alert System

In this case, we carefully analyze the distribution of average 24-hour differences leading up to February 02, 2021. This forms the core of our approach to trigger alerts in the year that follows. For the two critical accelerations, all six monitoring points consistently exceed the predefined thresholds, proving that our approach for setting the thresholds is robust. As in the case of the Sant'Andrea landslide, we have identified a recurring pattern where specific points sporadically surpass the established thresholds.

Once again, we observe a noteworthy reduction in the frequency of alerts as we extend the time intervals beyond a single hour. This trend is clearly illustrated in Figure 14, highlighting that a considerable portion of alerts occurs sporadically rather than consistently. The marked decline in alert occurrences as we lengthen the time intervals implies that many alerts do not signify enduring patterns but rather fleeting and sporadic (noisy) events.

Figure 15 displays the raw alerts produced by the system for each unstable monitoring point, without accounting for PiT or NP. As evident in the figure, certain monitoring locations display numerous incorrect alerts scattered throughout the entire testing dataset (but much less than in the Sant'Andrea landslide), with a concentration in the latter half of the year, particularly in 31, 32, and 33. However, in this case, the alerts are located specifically in correspondence with landslide accelerations. Figures 14, and 16 show again the effectiveness of the proposed combination between PT and NP, which can reduce the number of alerts, restricting them in correspondence of the most critical instances.

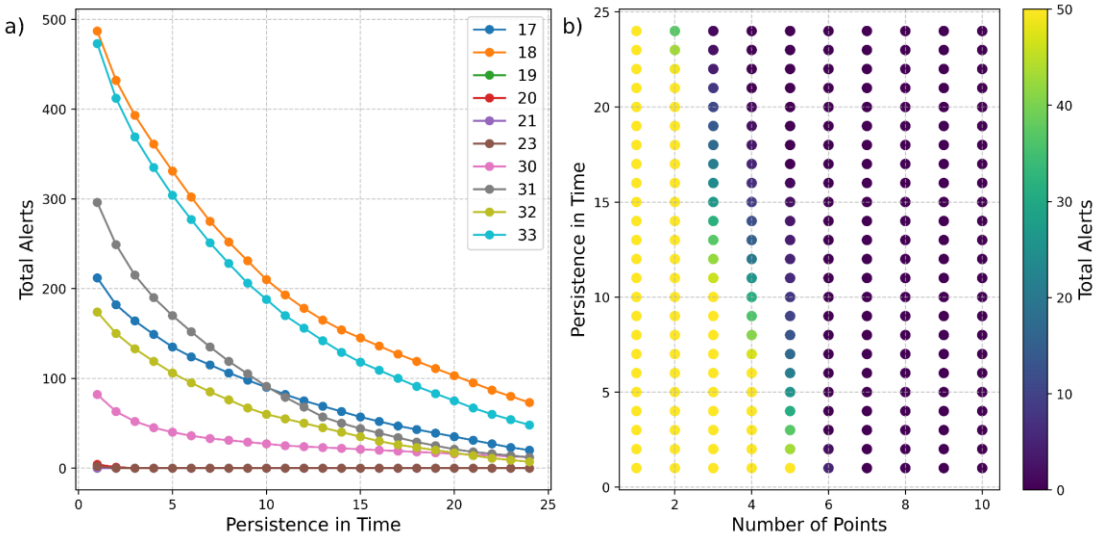

Figure 14. *a) Effect of the PiT on the number of times each monitoring point exceeds the threshold during the test year. b) Effect of the combination of PiT and the number of points that exceed the threshold simultaneously on the overall number of alerts the* LRSD *delivers.*

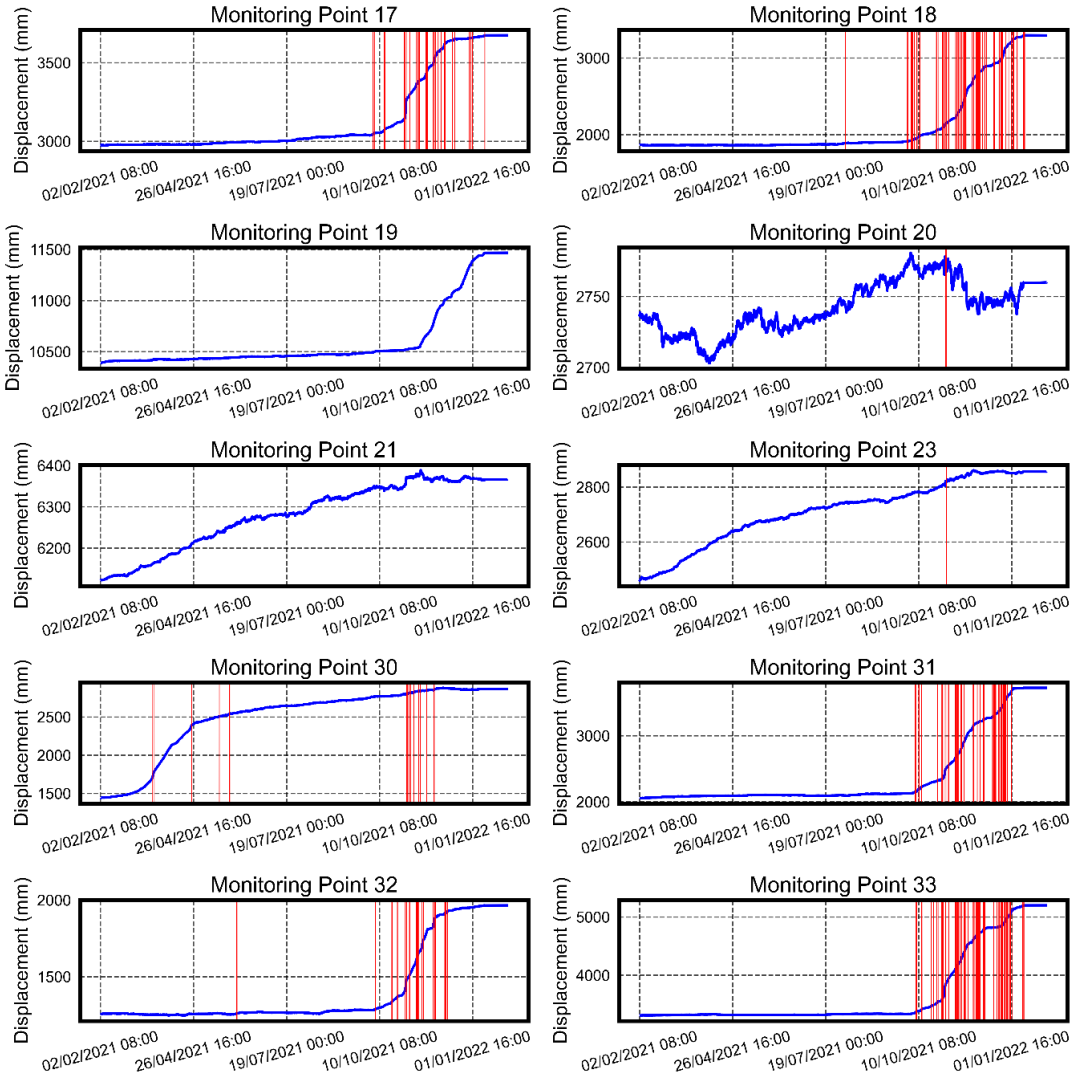

Figure 15. *Measured cumulative displacement (blue) and instances in which the threshold is exceeded for each monitoring point (red) located in the unstable landslide area.*

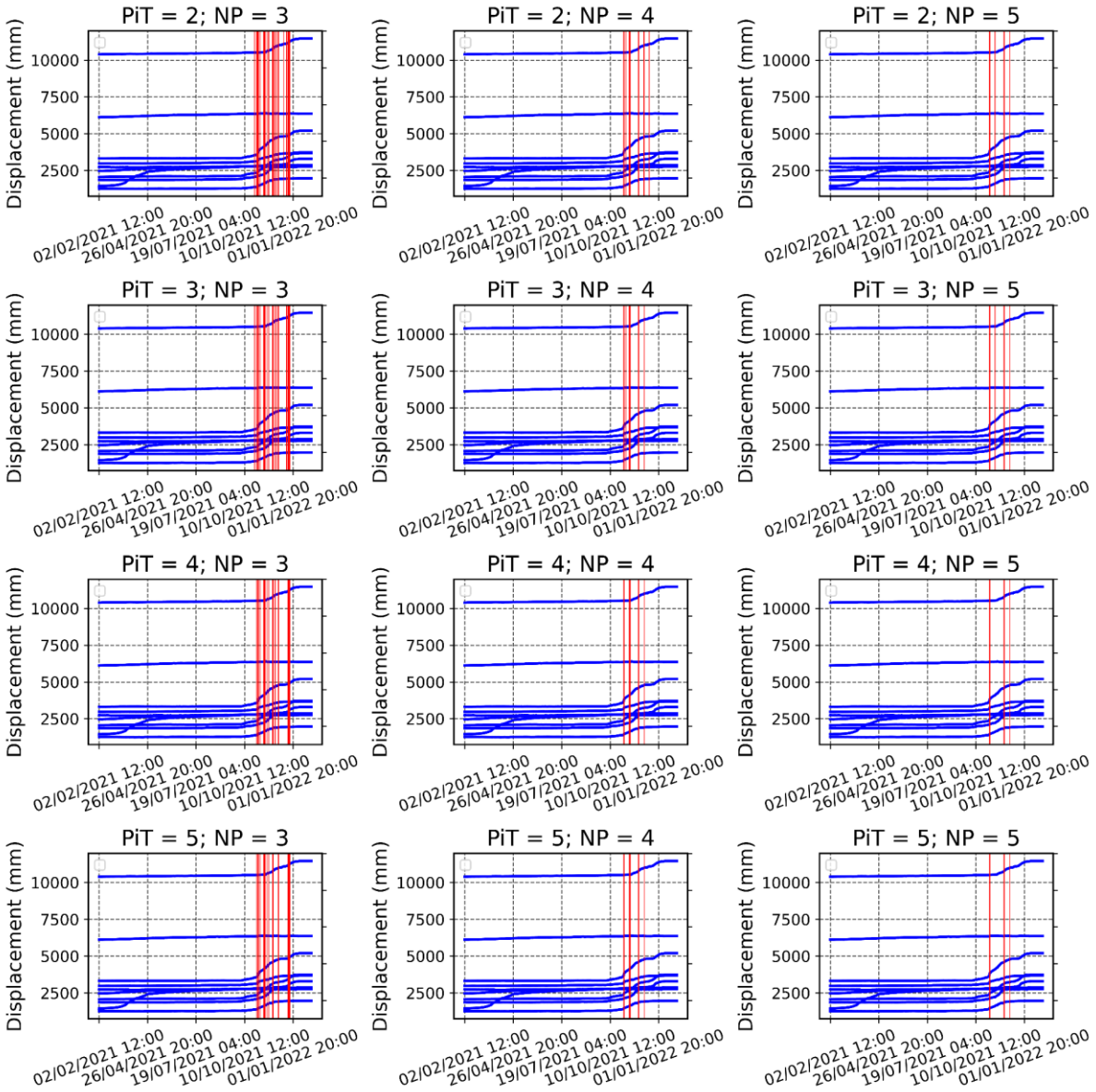

Figure 16. *Alerts (red) are delivered using 2, 3, 4, 5 as PiT and 3, 4, 5 as the number of points that exceed the threshold simultaneously. The measured cumulative displacement of the 10 points located in the unstable area is shown in blue.*

4.3 Veslemannen landslide

In the last year, the landslide behavior changed substantially showing two sudden strong accelerations and an overall increase in the displacement rate (Figure 6). At the end of the measured displacement, at 20:58 on the 5th of September 2019, the rock mass fails. This last year is used as a test for the LRSD since we want to evaluate and analyze the behavior of the proposed service as well in landslides with strong dynamic behavior and failure. The frequency of the time series analyzed is hourly, meaning that each test set, being one year is composed of 8760 time steps. As emphasized by Kristensen et al., (2021) the accelerations of the Veslemannen rockslide are, in part, initiated by the melting snow. Nevertheless, we exclude its modeling in this study to maintain the consistency of the data series frequency. It's worth noting that our system is designed to function effectively even when not all covariates are accessible, as demonstrated in this instance.

4.3.1 Model calibration and tuning

After the model is trained, it is used to predict the displacement of the 9 monitoring points on the landslide for 24h (of which 8 are consistently moving and 1 is stable), considering the measured values of the exogenous variable, rainfall, for the entire prediction window. The predicted displacement values can then be compared to the actual displacement values to assess the accuracy of the model. Similarly, to the Sant'Andrea study case, it is evident how the residuals increase in magnitude. especially in correspondence between the two major test year accelerations (see Figure 17).

The VECC model yielded optimal results with the following parameter settings: a detrending order of 0, lagged values of 4, and 'li' as a deterministic trend. This means that the displacement has a quadratic trend. The combined RMSE of the refined model across both the calibration and test sets amounts to 4.41 mm. Ablation analysis focusing on the external variable revealed that the most optimal outcomes are obtained when considering rainfall from the current day up to 27 days prior (with a 3-day shift interval). Nonetheless, in this scenario, the impact of changes in rainfall patterns on model performance exhibits some ambiguity. This ambiguity arises from the substantial influence of snowmelt on landslide accelerations. Consequently, the relationship between rainfall and displacement exhibits pronounced nonlinearity in certain instances. Nevertheless, we opted not to incorporate snowmelt into our model, as we placed a higher priority on maintaining the hourly time series frequency. In essence, modeling snowmelt would have necessitated transforming the data into daily intervals.

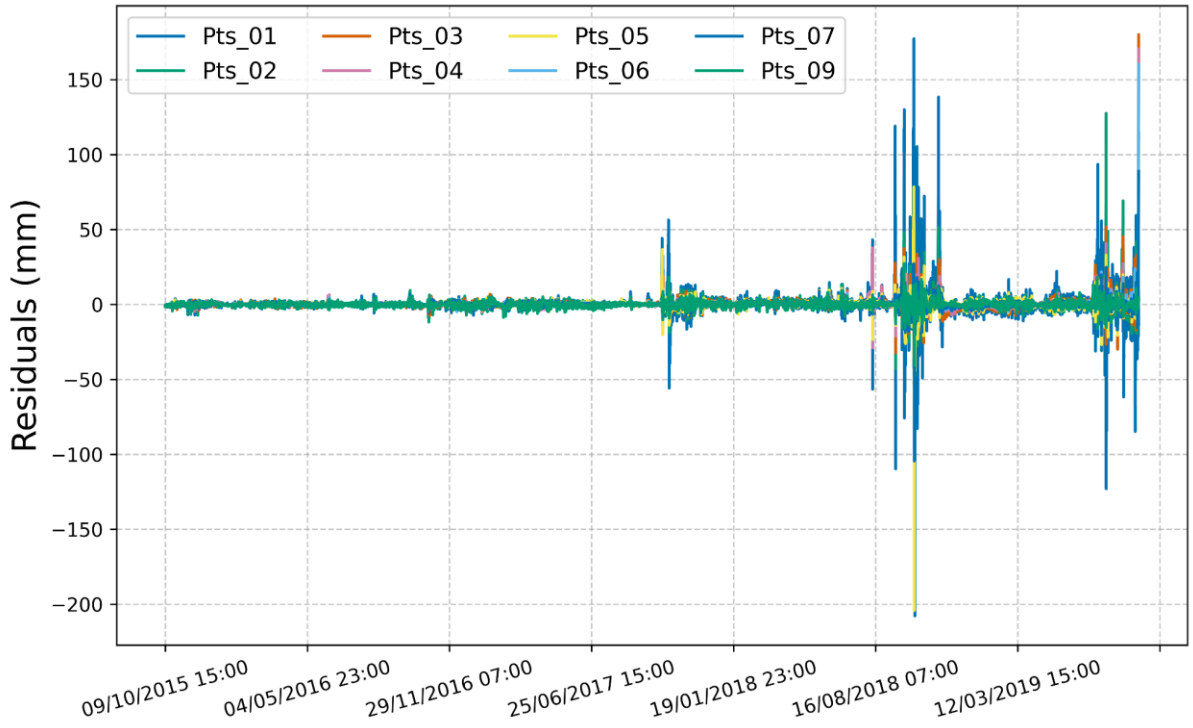

Figure 17. *Mean of residuals per 24h for each monitoring point located in the moving landslide area.*

4.3.2 Residual-based Landslide Alert System

As in the previous cases, we carefully analyze the distribution of average 24-hour residuals leading up to September 06, 2018. Figure 16 shows the instances in which each point individually exceeds the alert thresholds. As anticipated, the threshold levels are surpassed at the onset of significant sudden accelerations. The end of the presented displacement time series aligns with the instance of the rockslide failure. Monitoring point 01, responsible for measuring the highest overall displacement, does not breach the threshold before the failure event. Conversely, the remaining monitoring points situated within the area of failure promptly exceed the defined threshold.

A significant decrease in alert frequency is evident when extending PiT beyond a single hour. This pattern is depicted in Figure 18, emphasizing that a substantial portion of alerts occur intermittently rather than regularly.

Once again, the pronounced decrease in alert occurrences with longer time intervals suggests that many alerts do not represent persistent patterns, but instead, transient and irregular events.

Figure 19 displays the raw alerts produced by the system for each unstable monitoring point, without accounting for PiT or NP. As evident in the figure, certain monitoring locations display numerous incorrect alerts scattered throughout the entire testing dataset (but much less than in the Sant'Andrea landslide), with a concentration in the latter half of the year, particularly in 31, 32, and 33. However, in this case, the alerts are located specifically in correspondence with landslide accelerations. Figures 18 and 20 show the effectiveness of the proposed combination between PiT and NP, which can reduce the number of alerts, restricting them in correspondence with the most critical instances, and right before failure.

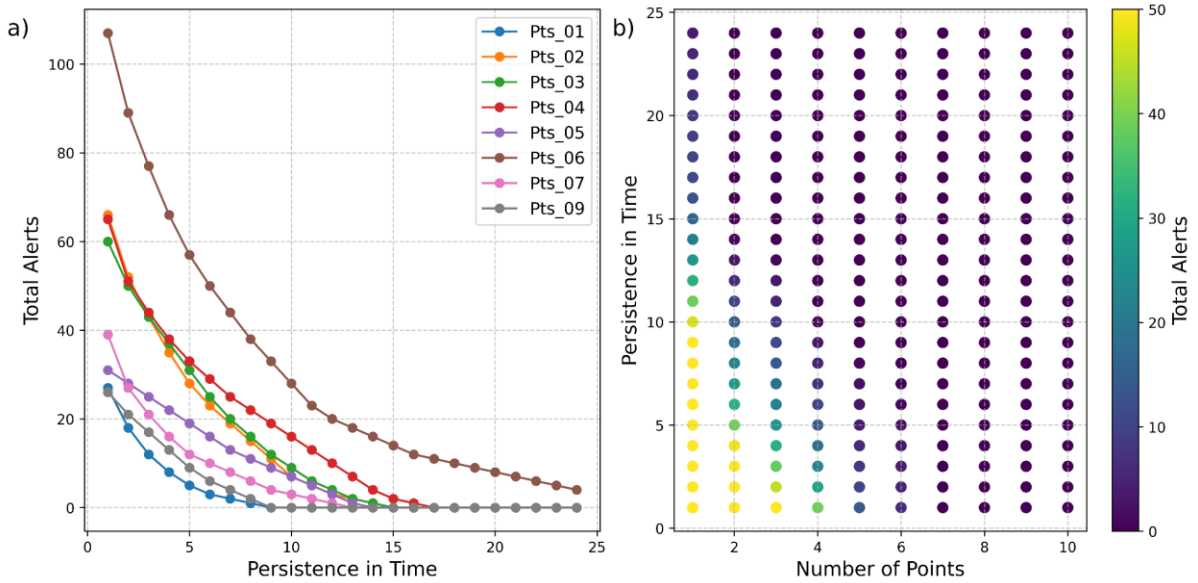

Figure 18. *a) Effect of the PiT on the number of times each monitoring point exceeds the threshold during the test year. b) Effect of the combination of PiT and the number of points that exceed the threshold simultaneously on the overall number of alerts the LRSD delivers.*

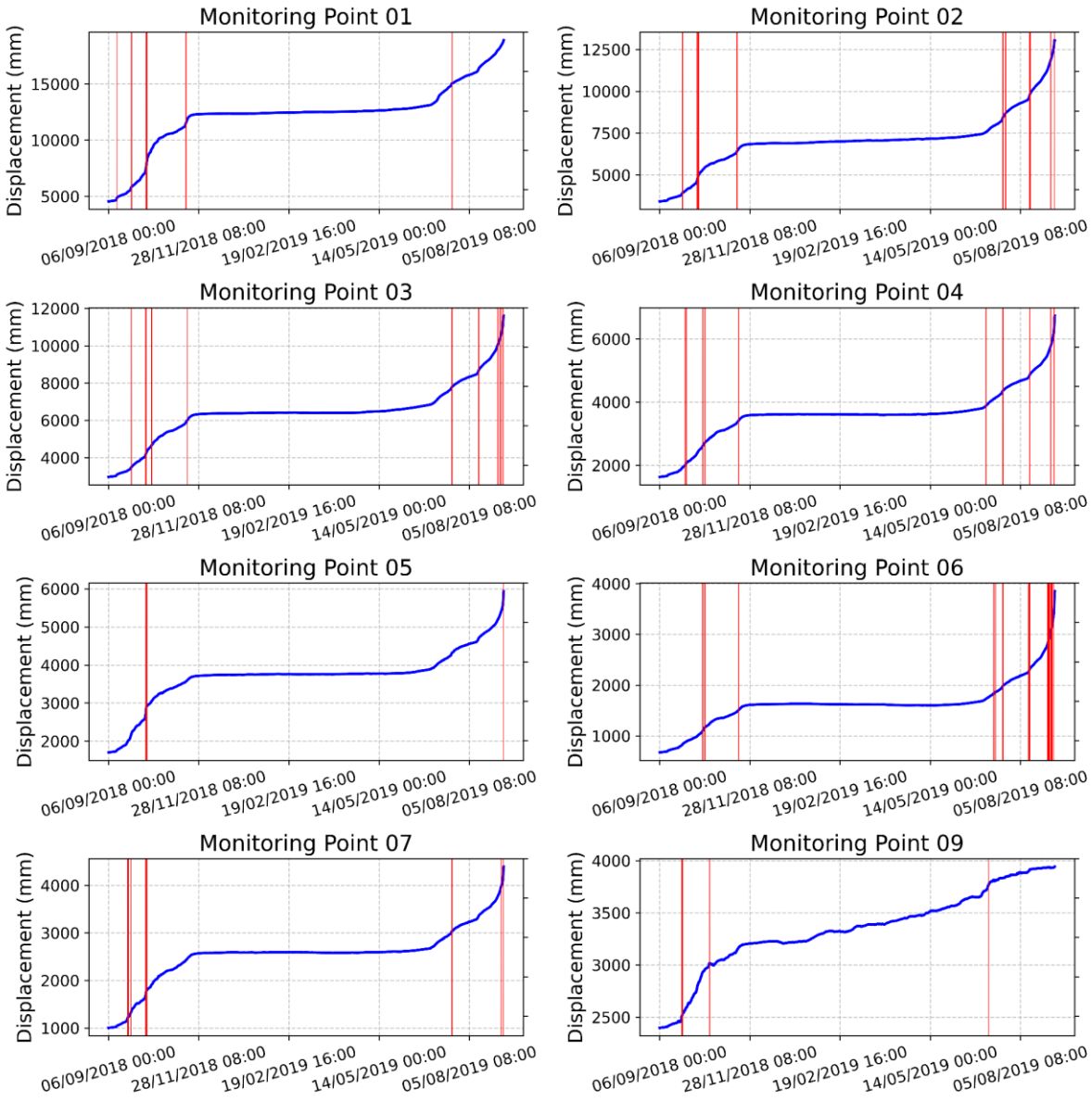

Figure 19. *Measured cumulative displacement (blue) and instances in which the threshold is exceeded for each monitoring point (red) located in the unstable landslide area.*

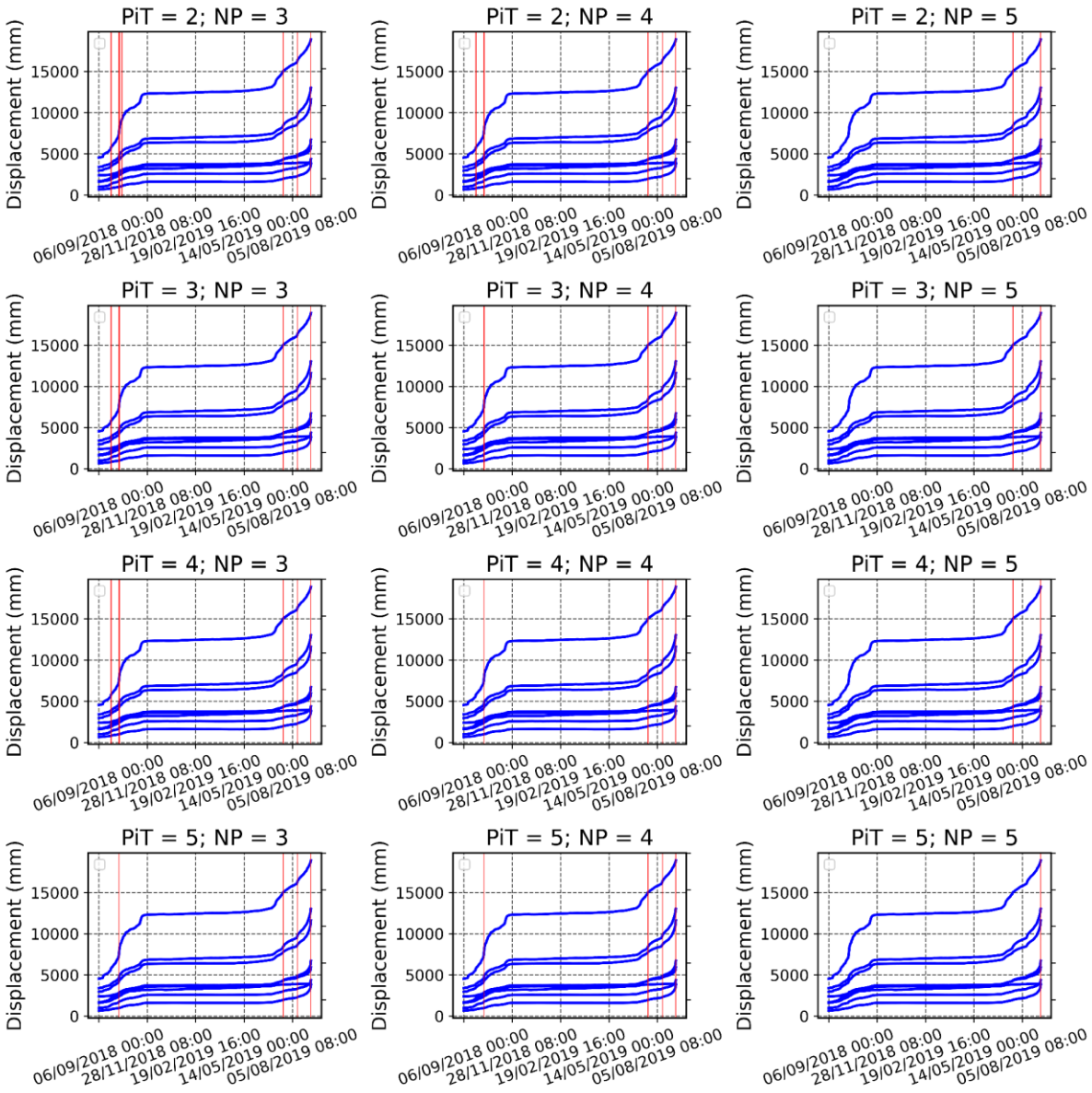

Figure 20. *Triggered alerts (red) using 2, 3, 4, 5 as PiT and 3, 4, 5 as the number of points (NP) that exceed the threshold simultaneously. The measured cumulative displacement of the 8 points located in the unstable area is shown in blue.*

6. Discussion

The proposed alert system is designed to capture the positive deviation from a given displacement regime to be coupled with classic warning systems such as displacement velocity thresholds, and incorporate the results into operational Lo-LEWS, to increase their redundancy and confidence in the resultant alert. The system assumes that the strong changes in the landslide behavior are the most critical instances. This means that if the landslide accelerates, and the prediction model can accurately predict the exact values of displacement at the same time and location, the alert is not sent. When the model can correctly predict the acceleration, it means that the spatial relationship among the displacements measured at all monitoring points, and their temporal relationship with rainfall remain invariant, for that instance, in comparison with their historical records. On the other hand, a small acceleration that is not correctly predicted is interpreted as a change in landslide behavior. Of course, as the approximation of the model is closer to reality the above-mentioned assumption can be considered correct. Any acceleration that is triggered by e.g. seismic or human activities will be considered as a deviation from the historical landslide regime. However, not every deviation from the modeled landslide regime would trigger an alert, since the threshold in the CDF can exclude most of the common residual values. Furthermore, we consider

it critical just when the model under-predicts the displacement, and not vice versa. We also remind that the VECC model is only able to capture linear relationships between the variables included in the modeling. However, it considers both spatial and transient nonstationary temporal dependencies between the variables, and, hence, the spatiotemporal relationship part of the stochastic phenomena. The focus of our paper revolves around modeling the displacement of the ground surface. However, we believe that extending this model to encompass subsurface displacement holds significant potential. Exploring the integration of subsurface and surface displacements in a unified model could also be of great interest.

Comparison with existing alert systems

In the considered landslides, there are established alert systems currently in operation. For the Pomarico landslide, the system comprises three velocity thresholds (set at 100, 200, and 300 mm/day for the main landslide body). These thresholds correspond to three distinct alert levels: *attention*, *pre-alarm*, and *alert* (Centro Protezione Civile Università degli Studi di Firenze, 2021). Within this system, only one *attention* alert is generated for the test year, with no *pre-alarm* or *alert* notifications issued. Interestingly, monitoring point 33 is the only one exceeding the threshold. This is exceeded at the time when the first alert is delivered by the proposed LRSD. Overall, the alerts produced by the existing system are fewer in number compared to those generated by the LRSD. Hence, in the context of the Pomarico landslide, it can be observed that the existing alert system exhibits lower sensitivity compared to the LRSD. The system in place for the Sant'Andrea landslide instead is slightly more complex. Two levels of *pre-alert* and one of *alert* can be delivered using average daily velocity thresholds, rainfall thresholds, and antecedent rainfall (Department of Geosciences, 2018). Here, during the test year, the population has been evacuated from the village twice. The first time was on Monday 7th December 2020 (https://www.amicodelpopolo.it/2020/12/07/perarolo-in-corso-levacuazione-delle-case-sotto-la-frana-della-busa-del-cristo/?doing_wp_cron=1697205920.0318601131439208984375) while the second time was on Monday 8th February 2021 (https://www.newsinquota.it/la-frana-si-muove-ancora-evacuate-tre-famiglie-a-perarolo/). In both cases the proposed alert system promptly delivers alerts. In the first case, the alert is triggered on Sunday 6th December (one day before), with a few hours of variability depending on the PiT and NP considered. In the second case, the proposed LRSD delivers alerts in the morning of Monday, starting from 08:00 a.m. for PiT = 1 to 01:00 p.m. when considering 5 hours of temporal persistence. In the Veslemannen rockslide study case, velocity threshold values for hazard levels were increased annually. Despite these adjustments, there were 16 evacuations in 2018 and 2019 due to rising velocities (Kristensen et al., 2021). In Figure 20, the proposed method visibly results in a notable decrease in the number of alerts. When both PiT and NP are set to 5, one alert is issued shortly before the occurrence of the failure, and no false alarms are displayed for the test set. However, in this case, the alert is sent at 8:00 p.m., just one hour before the failure. Nevertheless, as previously discussed, a shorter PiT allows for the alert to be delivered with a more substantial lead time (see Figures 18 and 20). Our work shares a conceptual similarity with the innovative approach introduced by Bernardie et al. in 2014, wherein a specific set of models is assumed to perfectly fit the normal landslide regime, and statistical methods are employed to establish thresholds based on the RMSE. Nonetheless, as their research primarily centers on forecasting rainfall-triggered accelerations, our approach consistently deviates from this emphasis. LRSD stands out by incorporating spatiotemporal relationships in the modeling phase and demonstrating adaptability across various study cases, showcasing its transferability. Notably, we go beyond by considering group dynamics, a fundamental aspect of the failure precursory theory. Additionally, we utilize raw historical residuals instead of RMSE, enabling us to distinguish between positive and negative deviations. This nuanced approach enhances the precision and depth of our analysis. However, aligned with their discoveries, our approach similarly demands substantial historical data, incorporating both displacement and meteorological parameters. For precise predictions, particularly for early warning applications, a continuous and systematically updated flow of data is imperative, coupled with efforts to minimize uncertainties.

Connections with the generic dynamics of the precursory failure regime in granular systems

Self-organized pattern formation (or collective motion) is a defining property of complex systems with a proven capacity to predict emergent behavior near critical transitions (Moon and Lu, 2015; Scheffer et al., 2009). This is particularly true for granular bodies in the stages leading up to catastrophic failure. In this context, comprehensive sampling plays a vital role in uncovering the unique dynamics of this precursory failure regime (PFR). Be it in a small-scale controlled laboratory sample or a large mountain slope, a specific dynamical signature in the form of a clustering pattern manifests in the observed motions in PFR (Tordesillas et al., 2021, 2018; Zhou et al., 2022).

In the absence of mitigative factors, a comprehensive characterization of this kinematic pattern has shown that as failure draws near, the stronger the pattern becomes, and the more it persists in space and time.

Of potential broad utility for landslide early warning is that this pattern and its spatiotemporal dynamics can be detected in the early stages of the precursory failure regime, well before the collapse in both engineered and natural slopes (Tordesillas et al., 2021, 2018; Zhou et al., 2022). That said, numerous monitoring points are needed to identify and track kinematic clustering. Having only a limited number of data series covering a monitoring area could make it challenging, or even impossible, to discern this pattern and its dynamics from the continuous monitoring data, unless relevant features that encode it can be found in the data and exploited. In the proposed LRSD, the persistence in time (PiT) and the number of points (NP) that exceed the threshold are two such features. As shown earlier, their incorporation into LRSD reduces the number of false alerts, thereby giving LRSD a key advantage: the capability to generate a useful warning with just a few monitoring points (time series data). Accordingly, we expect that the addition of more information into the data set through an increase in the monitoring points can only enhance the quality of the resultant alert from LRSD.

Operationality of the proposed alert framework

The design of the proposed alert system strictly considers its applicability in a real case: recall Graphical Abstract. One of the first requirements for operational alert systems is indeed the velocity with which the alert is sent. As described above, the VECC model can be trained and yield predictions within less than a second for all the monitoring points included in the modeling, with some variability depending upon the number of variables involved. Furthermore, the prediction framework can be adapted to the specific characteristics of the study case. After the parameters of the model are optimized, and the residual thresholds, PiT, and NP are defined the potential alert can be sent within a few seconds (again, with some degree of variability depending on the number of variables involved in the modeling). Other fundamental requirements of a reliable alert system are adaptability and transferability. Based on the case site, several features of the proposed framework can be modified and adapted. For instance, any trigger that can influence the landslide displacement can be included, such as seismic activity, temperature, or changes in the water level of the reservoir, if the landslide is located in an artificial reservoir context. Moreover, the method can be applied to different monitoring systems, as long as they can measure the landslide displacement with a constant temporal frequency. In this research, we show results for GB-SAR and RTS. Time series with higher (and lower) monitoring frequency can be used since the training and predicting window can be adapted as well. Moreover, PiT can be adapted to the specific necessity of the landslide case. If the tradeoff between false positives and scruples is strongly unbalanced towards the scruple, a small number of PiT can be used, and vice versa. Widening the PiT window will reduce the number of alarms, but it will increase the delay between the start of the anomalous acceleration and the triggering of the alert. Similarly, the NP can be adapted to the specific problem. If the volume related to a few monitoring points is dangerous a small number of NP can be used, and vice versa. Specific combinations of the monitoring points related to different predefined cinematic areas can be separately selected as well. Different levels of alerts can also be applied by considering a different number of points per alert, with a corresponding different degree of alert. Certainly, while directly incorporating geological and geotechnical characteristics of landslides into the model may present challenges, a viable solution lies in post-processing. This allows us to devise a system that indirectly integrates specific landslide features, such as predefined kinematic areas.

Certainly, every method comes with its limitations, and this is no exception. When the calibration set includes extreme residual values, the CDF changes drastically. As a consequence, the residual threshold risks are set too high, and very few alerts are sent afterward. Another crucial factor is the dependency on both the accuracy of model predictions and, of course, the quality of measured data. Variations in data quality, such as noise or missing data, introduce uncertainties that can impact the LRSD's accuracy. Moreover, the correlation between the accuracy of the proposed method and the number of monitoring points, as well as the time interval, is subject to variation depending on the specific characteristics of each landslide case. It's worth noting that an increased abundance of monitoring points and shorter time intervals undoubtedly enhances the accuracy and reliability of the approach, since the noise effect could be further reduced, and the redundancy of the system further increased. When addressing noisy data to minimize false alerts, fine-tuning the PiT parameter assumes critical importance. Nevertheless, as previously indicated, determining the ideal PiT settings is a case-by-case endeavor and demands thorough assessment for each scenario. Generally, noisier data would necessitate higher values for both PiT and NP. However, higher PiT values introduce delays in the alerting process.

Consequently, if we anticipate a failure with relatively brief precursory indicators, this could potentially impede timely detection.

5. Conclusions

We propose a robust and adaptive method for local landslide alert generation, to be coupled with existing alert systems. Grounded in material science and complex system dynamics, the LRSD considers multiple displacement time series to encode the "group dynamics," crucial for identifying pre-failure indications. The LRSD aims to improve conventional alert systems by detecting changes in expected displacement patterns, using anomalous accelerations as a key signal for alerts. Its adaptability to varying landslide contexts, rapid operational capabilities, and flexibility in adjusting parameters like PiT and NP enhances its potential for real-time applicability in diverse settings. The LRSD is intended for use in conjunction with current alert systems, like velocity thresholds. The concept is to maintain a high level of alerts through velocity thresholds for general safety, while LRSD aims to decrease the overall alert frequency. Instead, it provides heightened attention specifically for critical cases in which the system faces a regime shift. The LRSD informs you that the system is undergoing changes, indicating a transition, though it doesn't necessarily imply an impending landslide failure. This additional information is crucial for recognizing shifts in the system, which might lead to failure. The conjunction of information from both the velocity threshold and the LRSD creates an additional alert level. When both triggers initiate an alert, we can be more certain that we are closer to failure compared to relying on just one of them independently. Our results strongly suggest that incorporating LRSD into existing landslide early warning systems would greatly enhance their effectiveness.

Acknowledgments
The authors wish to thank the Veneto Region, Civil Protection Center of Veneto Region, and Veneto Strade for providing monitoring data and partially funding the research with the Grant “SUPPORTO SCIENTIFICO PER L’OTTIMIZZAZIONE, IMPLEMENTAZIONE E GESTIONE DEL SISTEMA DI MONITORAGGIO CON AGGIORNAMENTO DELLE SOGLIE DI ALLERTAMENTO DEL FENOMENO FRANOSO DI SANT’ANDREA – PERAROLO DI CADORE (BL)”, Edoardo Carraro for providing key information and reports about the Sant’Andrea landslide, Civil Protection Center of University of Florence and Ascanio Rosi for providing the displacement and rainfall data of Pomarico landslide, and Lene Kristensen and co-authors of Kristensen et al. (2021) for providing rainfall and displacement data for the Veslemannen rockslide.

References

Bernardie, S., Desramaut, N., Malet, J. P., Gourlay, M., Grandjean, G., 2015. Prediction of changes in landslide rates induced by rainfall. Landslides, 12, 481-494. https://doi.org/10.1007/s10346-014-0495-8

Blasques, F., Koopman, S.J., Nientker, M., 2022. A time-varying parameter model for local explosions. J Econom 227, 65–84. https://doi.org/10.1016/j.jeconom.2021.05.008

Brezzi, L., Carraro, E., Pasa, D., Teza, G., Cola, S., Galgaro, A., 2021. Post-Collapse Evolution of a Rapid Landslide from Sequential Analysis with FE and SPH-Based Models. Geosciences (Basel) 11, 364. https://doi.org/10.3390/geosciences11090364

Catani, F., Segoni, S., 2022. Prediction and Forecasting of Mass-Movements. Treatise on Geomorphology, 531–545. https://doi.org/10.1016/B978-0-12-818234-5.00099-7

Centro Protezione Civile Università degli Studi di Firenze. 2021. Monitoraggio e valutazione della frana di Pomarico (MT) tramite dati interferometrici da terra. Report of monitoring system. (in Italian)

Chen, Y.-C., 2017. A tutorial on kernel density estimation and recent advances. Biostat Epidemiol 1, 161–187. https://doi.org/10.1080/24709360.2017.1396742

Crosta, G.B., Agliardi, F., 2002. How to obtain alert velocity thresholds for large rockslides. Physics and Chemistry of the Earth, Parts A/B/C 27, 1557–1565. https://doi.org/10.1016/S1474-7065(02)00177-8

Crosta, G.B., Agliardi, F., Rivolta, C., Alberti, S., Dei Cas, L., 2017. Long-term evolution and early warning strategies for complex rockslides by real-time monitoring. Landslides 14, 1615–1632. https://doi.org/10.1007/s10346-017-0817-8

Department of Geosciences, University of Padova. 2018. Frana di Sant'Andrea, Perarolo di Cadore (BL). Final technical report. (in Italian)

Dick, G.J., Eberhardt, E., Cabrejo-Liévano, A.G., Stead, D., Rose, N.D., 2015. Development of an early-warning time-of-failure analysis methodology for open-pit mine slopes utilizing ground-based slope stability radar monitoring data. Canadian Geotechnical Journal 52, 515–529. https://doi.org/10.1139/cgj-2014-0028

Doglioni, A., Casagli, N., Nocentini, M., Sdao, F., Simeone, V., 2020. The landslide of Pomarico, South Italy, occurred on January 29th 2019. Landslides 17, 2137–2143. https://doi.org/10.1007/s10346-020-01455-x

Du, J., Yin, K., Lacasse, S., 2013. Displacement prediction in colluvial landslides, Three Gorges Reservoir, China. Landslides 10, 203–218. https://doi.org/10.1007/s10346-012-0326-8

Festa, D., Novellino, A., Hussain, E., Bateson, L., Casagli, N., Confuorto, P., Del Soldato, M., Raspini, F., 2023. Unsupervised detection of InSAR time series patterns based on PCA and K-means clustering. International Journal of Applied Earth Observation and Geoinformation 118, 103276. https://doi.org/10.1016/j.jag.2023.103276

Froude, M.J., Petley, D.N., 2018. Global fatal landslide occurrence from 2004 to 2016. Natural Hazards and Earth System Sciences 18, 2161–2181. https://doi.org/10.5194/nhess-18-2161-2018

Fukuzono, T., 1985. A new method for predicting the failure time of slope. Proceedings, 4th Int'l. Conference and Field Workshop on Landslides, 145-150. https://doi.org/10.3313/jls1964.22.2_8

Gao, Y., Chen, X., Tu, R., Chen, G., Luo, T., Xue, D., 2022. Prediction of Landslide Displacement Based on the Combined VMD-Stacked LSTM-TAR Model. Remote Sens (Basel) 14, 1164. https://doi.org/10.3390/rs14051164

Gouriéroux, C., Zakoïan, J.-M., 2017. Local Explosion Modelling by Non-Causal Process. J R Stat Soc Series B Stat Methodol 79, 737–756. https://doi.org/10.1111/rssb.12193

Han, H., Shi, B., Zhang, L., 2021. Prediction of landslide sharp increase displacement by SVM with considering hysteresis of groundwater change. Eng Geol 280, 105876. https://doi.org/10.1016/j.enggeo.2020.105876

Hilger, P., Hermanns, R. L., Gosse, J. C., Jacobs, B., Etzelmüller, B., Krautblatter, M., 2018. Multiple rock-slope failures from Mannen in Romsdal Valley, western Norway, revealed from Quaternary geological mapping and 10Be exposure dating. The Holocene, 28(12), 1841-1854. https://doi.org/10.1177/0959683618798165

Intrieri, E., Gigli, G., Casagli, N., Nadim, F., 2013. Brief communication "Landslide Early Warning System: toolbox and general concepts" Natural Hazards and Earth System Sciences 13, 85–90. https://doi.org/10.5194/nhess-13-85-2013

Intrieri, E., Gigli, G., Mugnai, F., Fanti, R., Casagli, N., 2012. Design and implementation of a landslide early warning system. Eng Geol 147–148, 124–136. https://doi.org/10.1016/j.enggeo.2012.07.017

Jiang, Z., Chen, H., 2022. A new early warning method for dam displacement behavior based on non-normal distribution function. Water Science and Engineering 15, 170–178. https://doi.org/10.1016/j.wse.2022.04.001

Ju, N., Huang, J., He, C., Van Asch, T. W. J., Huang, R., Fan, X., ... Wang, J., 2020. Landslide early warning, case studies from Southwest China. Engineering Geology, 279, 105917. https://doi.org/10.1016/j.enggeo.2020.105917

Kawamura, K., 1985. Methodology for landslide prediction. International conference on soil mechanics and foundation engineering, 11, 1155-1158.

Kristensen, L., Czekirda, J., Penna, I., Etzelmüller, B., Nicolet, P., Pullarello, J.S., Blikra, L.H., Skrede, I., Oldani, S., Abellan, A., 2021. Movements, failure and climatic control of the Veslemannen rockslide, Western Norway. Landslides 18, 1963–1980. https://doi.org/10.1007/s10346-020-01609-x

Lacroix, P., Handwerger, A. L., Bièvre, G., 2020. Life and death of slow-moving landslides. Nature Reviews Earth & Environment, 1(8), 404-419. https://doi.org/10.1038/s43017-020-0072-8

Leinauer, J., Weber, S., Cicoira, A., Beutel, J., Krautblatter, M., 2023. An approach for prospective forecasting of rock slope failure time. Communications Earth & Environment, 4(1), 253. https://doi.org/10.1038/s43247-023-00909-z

Liu, Z., Shao, J., Xu, W., Chen, H., Shi, C., 2014. Comparison on landslide nonlinear displacement analysis and prediction with computational intelligence approaches. Landslides 11, 889–896. https://doi.org/10.1007/s10346-013-0443-z

Lütkepohl, H, 2005. New introduction to multiple time series analysis. Springer Science & Business Media.

Marmoni, G.M., Martino, S., Censi, M., Menichetti, M., Piacentini, D., Scarascia Mugnozza, G., Torre, D., Troiani, F., 2023. Transition from rock mass creep to progressive failure for rockslide initiation at Mt. Conero (Italy). Geomorphology 437, 108750. https://doi.org/10.1016/j.geomorph.2023.108750

Moon, H., Lu, T.-C., 2015. Network Catastrophe: Self-Organized Patterns Reveal both the Instability and the Structure of Complex Networks. Sci Rep 5, 9450. https://doi.org/10.1038/srep09450

Nava, L., Carraro, E., Reyes-Carmona, C., Puliero, S., Bhuyan, K., Rosi, A., Monserrat, O., Floris, M., Meena, S.R., Galve, J.P., Catani, F., 2023. Landslide displacement forecasting using deep learning and monitoring data across selected sites. Landslides 20. https://doi.org/10.1007/s10346-023-02104-9

Palmer, J., 2017. Creeping earth could hold secret to deadly landslides. Nature, 548, 384–386. https://doi.org/10.1038/548384a

Pecoraro, G., Calvello, M., Piciullo, L., 2019. Monitoring strategies for local landslide early warning systems. Landslides 16, 213–231. https://doi.org/10.1007/s10346-018-1068-z

Perrone, A., Canora, F., Calamita, G., Bellanova, J., Serlenga, V., Panebianco, S., Tragni, N., Piscitelli, S., Vignola, L., Doglioni, A., Simeone, V., Sdao, F., Lapenna, V., 2021. A multidisciplinary approach for landslide residual risk assessment: the Pomarico landslide (Basilicata Region, Southern Italy) case study. Landslides 18, 353–365. https://doi.org/10.1007/s10346-020-01526-z

Petley, D.N., Allison, R.J., 1997. The mechanics of deep-seated landslides. Earth Surf Process Landf 22, 747–758. https://doi.org/https://doi.org/10.1002/(SICI)1096-9837(199708)22:8<747::AID-ESP767>3.0.CO;2-#

Phillips, P.C.B., Shi, S., 2020. Real time monitoring of asset markets: Bubbles and crises. pp. 61–80. https://doi.org/10.1016/bs.host.2018.12.002

Phillips, P.C.B., Wu, Y., Yu, J., 2011. EXPLOSIVE BEHAVIOR IN THE 1990s NASDAQ: WHEN DID EXUBERANCE ESCALATE ASSET VALUES? Int Econ Rev (Philadelphia) 52, 201–226. https://doi.org/10.1111/j.1468-2354.2010.00625.x

Qian, G., Tordesillas, A., Zheng, H., 2021. Landslide Forecast by Time Series Modeling and Analysis of High-Dimensional and Non-Stationary Ground Motion Data. Forecasting 3, 850–867. https://doi.org/10.3390/forecast3040051

Saintot, A., Oppikofer, T., Derron, M.-H., Henderson, I., 2012. Large gravitational rock slope deformation in Romsdalen valley (Western Norway). Revista De La Asociación Geológica Argentina, 69(3), 354-371. Retrieved from https://revista.geologica.org.ar/raga/article/view/521

Segalini, A., Valletta, A., Carri, A., 2018. Landslide time-of-failure forecast and alert threshold assessment: A generalized criterion. Engineering geology, 245, 72-80. https://doi.org/10.1016/j.enggeo.2018.08.003

Segoni, S., Rossi, G., Rosi, A., Catani, F., 2014. Landslides triggered by rainfall: A semi-automated procedure to define consistent intensity–duration thresholds. Comput Geosci 63, 123–131. https://doi.org/10.1016/j.cageo.2013.10.009

Scheffer, M., Bascompte, J., Brock, W.A., Brovkin, V., Carpenter, S.R., Dakos, V., Held, H., van Nes, E.H., Rietkerk, M., Sugihara, G., 2009. Early-warning signals for critical transitions. Nature 461, 53–59. https://doi.org/10.1038/nature08227

Tordesillas, A., Kahagalage, S., Campbell, L., Bellett, P., Intrieri, E., Batterham, R., 2021. Spatiotemporal slope stability analytics for failure estimation (SSSAFE): linking radar data to the fundamental dynamics of granular failure. Sci Rep 11, 9729. https://doi.org/10.1038/s41598-021-88836-x

Tordesillas, A., Zhou, Z., Batterham, R., 2018. A data-driven complex systems approach to early prediction of landslides. Mech Res Commun 92, 137–141. https://doi.org/10.1016/j.mechrescom.2018.08.008

Tordesillas, A., et al., 2023. Augmented intelligence forecasting and what-if-scenario analytics with quantified uncertainty for big real-time slope monitoring data. (manuscript in review)

Voight, B., 1988. A method for prediction of volcanic eruptions. Nature, 332, 125-130.

Wang, H., Qian, G., Tordesillas, A., 2020. Modeling big spatio-temporal geo-hazards data for forecasting by error-correction cointegration and dimension-reduction. Spat Stat 36, 100432. https://doi.org/10.1016/j.spasta.2020.100432

Wang, Y., Tang, H., Wen, T., Ma, J., 2019. A hybrid intelligent approach for constructing landslide displacement prediction intervals. Appl Soft Comput 81, 105506. https://doi.org/10.1016/j.asoc.2019.105506

Ye, X., Zhu, H., Wang, J., Zhang, Q., Shi, B., Schenato, L., Pasuto, A., 2022. Subsurface Multi-Physical Monitoring of a Reservoir Landslide With the Fiber-Optic Nerve System. Geophys Res Lett 49. https://doi.org/10.1029/2022GL098211

Zhang, W., Li, H., Tang, L., Gu, X., Wang, Luqi, Wang, Lin, 2022. Displacement prediction of Jiuxianping landslide using gated recurrent unit (GRU) networks. Acta Geotech 17, 1367–1382. https://doi.org/10.1007/s11440-022-01495-8

Zhang, X., Li, P., 2014. Lithological mapping from hyperspectral data by improved use of spectral angle mapper. International Journal of Applied Earth Observation and Geoinformation 31, 95–109. https://doi.org/10.1016/j.jag.2014.03.007

Zheng, H., Qian, G., Tordesillas, A., 2023. Modelling High-Dimensional Time Series with Nonlinear and Nonstationary Phenomena for Landslide Early Warning and Forecasting, in: ITISE 2023. MDPI, Basel Switzerland, p. 21. https://doi.org/10.3390/engproc2023039021

Zhou, C., Yin, K., Cao, Y., Intrieri, E., Ahmed, B., Catani, F., 2018. Displacement prediction of step-like landslide by applying a novel kernel extreme learning machine method. Landslides 15, 2211–2225. https://doi.org/10.1007/s10346-018-1022-0

Zhou, S., Tordesillas, A., Intrieri, E., Di Traglia, F., Qian, G., Catani, F., 2022. Pinpointing Early Signs of Impending Slope Failures From Space. J Geophys Res Solid Earth 127. https://doi.org/10.1029/2021JB022957

Zhu, C.H., Hu, G.D., 2012. Time Series Prediction of Landslide Displacement Using SVM Model: Application to Baishuihe Landslide in Three Gorges Reservoir Area, China. Applied Mechanics and Materials 239–240, 1413–1420. https://doi.org/10.4028/www.scientific.net/AMM.239-240.1413

Zvelebill, J., Moser, M., 2001. Monitoring based time-prediction of rock falls: Three case-histories. Physics and Chemistry of the Earth, Part B: Hydrology, Oceans and Atmosphere, 26, 2, 159-167. https://doi.org/10.1016/S1464-1909(00)00234-3